

UNCLASSIFIED

AD NUMBER

AD522005

CLASSIFICATION CHANGES

TO: unclassified

FROM: confidential

LIMITATION CHANGES

TO:

Approved for public release, distribution unlimited

FROM:

AUTHORITY

ONR ltr., Ser 93/804, 26 Aug 1998; Same

THIS PAGE IS UNCLASSIFIED

UNCLASSIFIED



AD NUMBER

AD 522 005

CLASSIFICATION CHANGES

TO CONFIDENTIAL

FROM SECRET

AUTHORITY

OCA; JULY 31, 1984

THIS PAGE IS UNCLASSIFIED

AD 522005

THIRD QUARTERLY TECHNICAL STATUS REPORT
HIGH-P WAVE CO LASER (H)

Prepared by
Research and Technology Center
Laser Technology Laboratories

This document contains information affecting the national defense of the United States, within the meaning of the Espionage Laws, Title 18, U.S.C., Sections 793 and 794, the transmission or revelation of which in any manner to an unauthorized person is prohibited by law.

Approved for Release: A.C. 0043

Approved by
DEFENSE RESEARCH PROJECTS AGENCY
AREA OFFICE NO. 1806

Approved by
OFFICE OF NAVAL RESEARCH
NAVY OFFICE 417

EXPIRES: AS 17 YEAR DATE
WAVE, NOT AUTOMATICALLY
EXPIRES: 100 OF 100.10

DDIC
PROFORMED
SEP 7 52
REGULATED

RESEARCH CORPORATION

DEFENSE RESEARCH AGENCY

WASHINGTON, D.C.

ALL CONTROL
NO. 21819

REPRODUCTION QUALITY NOTICE

This document is the best quality available. The copy furnished to DTIC contained pages that may have the following quality problems:

- **Pages smaller or larger than normal.**
- **Pages with background color or light colored printing.**
- **Pages with small type or poor printing; and or**
- **Pages with continuous tone material or color photographs.**

Due to various output media available these conditions may or may not cause poor legibility in the microfiche or hardcopy output you receive.

If this block is checked, the copy furnished to DTIC contained pages with color printing, that when reproduced in Black and White, may change detail of the original copy.

NOTICE

The views and conclusions contained in this document are those of the authors and should not be interpreted as necessarily representing the official policies, either expressed or implied, of the Advanced Research Projects Agency or the U. S. Government.



NLSD 72-14R

**THIRD QUARTERLY TECHNICAL STATUS REPORT
HIGH POWER CO LASER (U)**

**Research and Technology Center
Laser Technology Laboratories**

July 1972

Contract No. N00014-72-C-0043

**GROUP THREE
DOWNGRADED AT 12 YEAR
INTERVALS; NOT AUTOMATICALLY
DECLASSIFIED OOD OIR 5200.10**

**Sponsored by
ADVANCED RESEARCH PROJECTS AGENCY
ARPA ORDER NO. 1806**

**Monitored by
OFFICE OF NAVAL RESEARCH
CODE 421**

**DDC
RECEIVED
SEP 7 1972
D.**

This document contains information affecting the National Defense of the United States, within the meaning of the Espionage Laws, Title 18, U.S.C. Sections 793 and 794, the transmission or revelation of which in any manner to an unauthorized person is prohibited by law.

CNP 2491

Copy



**DDC CONTROL
NO. 21819**

UNCLASSIFIED

PROGRAM IDENTIFICATION (U)

ARPA Order No. : 1806

Program Code No. : 1E90

Name of Contractor: Northrop Corporation

Effective date of contract: 1 August 1971 - 30 September 1972

Amount of Contract: \$1,331,273.00

Contract No. : N00014-72-C-0043

Program Manager: Dr. G. Hasserjian
(213) 675-4611, Ext 4861

Project Scientist: Dr. M. M. Mann
(213) 675-4611, Ext 2821

Scientific Officer: Director, Physics Program
Physical Sciences Division
Office of Naval Research
Department of Navy
800 North Quincy
Arlington, Virginia 22217

Disclaimer: The views and conclusions contained in this document are those of the authors and should not be interpreted as necessarily representing the official policies, either expressed or implied, of the Advanced Research Projects Agency or the U. S. Government.

TABLE OF CONTENTS (U)

1.0	SUMMARY	1
2.0	THE KINETIC MODEL AND VIBRATIONAL CROSS RELAXATION RATES	5
2.1	Plasma Characteristics	5
2.2	VV Cross Relaxation Rates	7
2.3	Rate Constant Measurements	9
3.0	E-BEAM STABILIZED DISCHARGE LASER RESULTS	34
3.1	Experimental Description	34
3.2	Experimental Results	39
4.0	DESIGN AND CALIBRATION OF A WATER VAPOR CELL FOR LINE SELECTION	48
4.1	The Absorption Cell	48
4.2	Calibration and Absorption Measurements	53
5.0	AREA CATHODE E-GUN DEVELOPMENT	57
5.1	Impregnated Cathode Characteristics	57
5.2	Prototype Tests	58
5.3	Large Area Cathode E-gun	67
5.4	Power Supplies	78
6.0	REFERENCES	79

[REDACTED]

1.0 SUMMARY

(S) The purpose of this program is to develop, on an approximately two year time scale, a 1 - 2 MW average power, variable pulse repetition rate diffraction-limited CO laser operating at an electrical efficiency of 50% or more. The work covered in this contract involves the design of intermediate power CO laser devices, the development of the required CO laser technology, and the construction of an intermediate power CO laser device.

(U) This program encompasses, on a best effort basis, the following major tasks:

(U) 1. The development of both steady state and transient kinetic models in order that realistic theoretical predictions of high energy device characteristics can be made.

(U) 2. Measurements of basic parameters of the CO laser at low pressures including: gain, saturation intensity, rates of vibrational cross-relaxation between CO molecules, transfer rates of CO and N₂, discharge characteristics, and spectral characteristics.

(U) 3. Measurements and characterization of a high pressure E-beam excited pulsed laser to experimentally determine transient operating parameters for high energy extraction.

(U) 4. The design and construction of a 500J/pulse diffraction-limited CO laser oscillator.

(U) 5. The development of mirror fabrication techniques for pulsed operation.

[REDACTED]

(U) 6. The development of line selection techniques for controlling the oscillator spectral output.

(S) 7. Preliminary design of a 20KJ/pulse diffraction-limited CO laser oscillator-amplifier system.

(U) The most significant accomplishments of the last quarter were: A series of experimental measurements of the near resonant CO vibrational cross relaxation rates with a three laser experimental technique, the introduction of the modified V-V rates into the kinetic model (according to the Jeffers and Kelley theory¹), parametric investigation of the E-beam stabilized discharge laser at low temperatures, and the operation of the laser at 25 - 40% efficiency with an output corresponding to 100 - 200 J/pulse per liter-atmosphere. Satisfactory progress has also been made in the other tasks of the program listed above. Technical reports and published papers (see references 2 through 13) contain detailed description of work completed on this program, and a review of the highlights of the activity of the last quarter is presented here.

(U) Previous calculations with the kinetic model of the CO laser compared very favorably with cw laser small signal gain measurements at room and cryogenic temperatures, and pulsed E-beam laser output measurements at room temperature. More recent measurements of transient characteristics of both the E-beam laser at low temperature and a cw laser (perturbed by a saturating pulse) indicate that near resonant V-V rates are considerably higher than that predicted by the SSH theory. Considerable effort has been devoted to more detailed measurements and modification of the rates to obtain consistent agreement between theory and experiment over a wide range of parameters. To date, this has not yet been possible. However, a

UNCLASSIFIED

give sufficient absorption and line width to achieve rotational line selection (and possibly some degree of vibrational band selection) with a pulsed device.

(U) The design of a 10 liter device, for near diffraction limited operation, has been completed and its construction is in progress. A review of the work done on the electron gun design for this device, including model tests and the full scale gun, is described in Section 5.0.

UNCLASSIFIED

2.0 THE KINETIC MODEL AND VIBRATIONAL CROSS RELAXATION RATES

(U) The analytical molecular kinetic model, described in greater detail in previous reports,^{5,11,14} was developed to predict the radiative characteristics of electrically excited cw or pulsed CO laser devices. The computer program for this model was constructed to calculate vibrational population and temperature distributions, gains, saturation characteristics, energy transfer and extraction rates, conversion efficiencies, output intensities, and spectral distributions as a function of time. There is a continuing effort made to compare predictions of this model with a variety of experimental results obtained from small-signal gain measurements, vibrational cross-relaxation data, and E-beam laser operation. Recently, this model was revised to incorporate newer theories of VV rates, as well as to adjust plasma characteristics as a function of time to correspond to experimentally observed behavior in the E-beam device.

2.1 Plasma Characteristics. (U) The present model assumes that the electron distribution can be described by a Boltzmann function, characterized by an electron temperature T_e . Electrical excitation rates from the ground state to the first eight vibrational levels in CO or N₂ are obtained by integrating this distribution over the experimentally measured Schulz cross sections. For the purpose of the molecular kinetic calculations, the plasma is characterized completely by specifying the electron density and temperature, and previously, the computer code assumed them to be fixed parameters. The choice of suitable values of these constants was guided by independent plasma calculations⁶ for the

UNCLASSIFIED

electron density and extrapolation of the results of Nighan,¹⁵ which give average electron energy as a function of E/N. Final adjustments were made, if necessary, to produce agreement with experimentally measured electrical excitation power per unit volume.

(U) There is, however, experimental evidence from investigations of the high pressure pulsed electric CO laser which suggests that electrical excitation as a function of time may not be adequately described by a fixed electron temperature, or fixed electron number density. Experimental data on sustainer voltage and sustainer current suggests that the electrical input excitation power is more accurately described by a rise time t_r and fall time t_f :

$$W^e(t) = P_0 (1 - e^{-t/t_r}) e^{-t/t_f}.$$

Plasma calculations⁶ of the electron number density show that there is a turn-on time required to attain a steady state value n_e^0 , so the rise time in the sustainer current is attributed to that effect, and it is assumed that

$$n_e(t) = n_e^0 (1 - e^{-t/t_r}).$$

The physical origin of the fall time t_f is the drop in the sustainer voltage due to the discharge of the capacitor bank. Since $W^e(t)$ also depends upon the molecular distribution $n_k(t)$ ($k = 0, 1, 2, \dots$), the electrical temperature must also be a slowly varying function of time. The physical reason for this is that, as the molecular levels become vibrationally "hot," less electrical energy can be transferred if T_e remains fixed. I. e., the inelastic molecular vibrational excitation collisions become less efficient for cooling the electron gas, and thus, T_e must rise. The computer code is now

UNCLASSIFIED

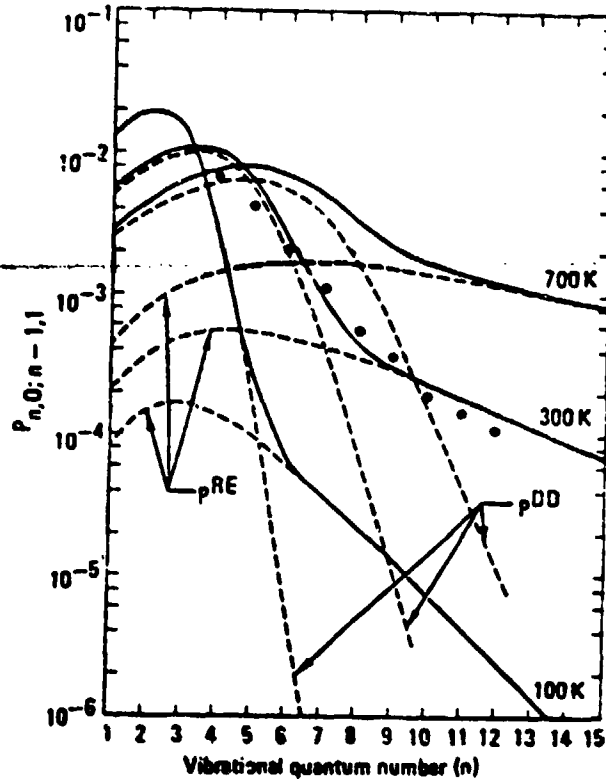
... of the plasma characteristics n_e and T_e to account for these effects.

(1) Although a completely self-consistent analysis should attempt to treat both the molecular and plasma kinetics on an equal basis as a coupled system, there is much useful information that can be obtained by analyzing them independently, and this continues to be the philosophy of the present approach. Future efforts may be necessary to extend the molecular kinetic analysis to include the electron kinetics of the plasma properly.

2.2 VV Cross-Relaxation Rates. (U) In the initial formulation of the present kinetic model, the rate matrix for the near-resonant VVT exchange collisions was constructed using modified SSH theory, with a forced fit to the rate for $(1, 0 \rightleftharpoons 0, 1)$ given by Yardley,¹⁶ who inferred it from overall relaxation time for $\Delta v = 2$ fluorescence decay. In the present version of the model, the theory for the VVT rates has been revised. The formulation of these rates for (CO, CO) collisions is now based on long range dipole-dipole forces and short range exponential repulsive forces, following the work of Jeffers and Kelley,¹ who showed that such a theory compares favorably with experimental data of Hancock and Smith.¹⁷ Probabilities for the endothermic react $(n, 0 \rightarrow n-1, 1)$ are shown for a variety of kinetic temperatures in Figure 2.1.

UNCLASSIFIED

UNCLASSIFIED



(U) Figure 2.1. CO-CO VV probabilities from the theory of Jeffers and Kelley. (U)

(U) This theory contains essentially no adjustable parameters, and permits the calculation of the entire matrix of VVT rates as a function of the kinetic and rotational temperatures. There are, however, several serious problems associated with this theory. First of all, as is the case for several such theories, probabilities along and near the diagonal (i. e., for the highly resonant collisions) become comparable and greater than unity for only modest values of v (≥ 10), and must be truncated somehow.

UNCLASSIFIED

UNCLASSIFIED

Secondly, the theory fails to support the experimentally measured data at low temperatures ($\sim 100^{\circ}\text{K}$) recently reported by Wittig and Smith.¹⁸ Finally, calculations for cw population distributions using this theory to compare with small-signal gain measurements in low pressure systems seem to produce anomalously high population densities in the higher vibrational levels, unless sufficient truncation is introduced in the VVT rates in these levels. However, comparison of results obtained using this theory produced reasonable agreement with experimental results obtained from the high pressure E-beam pulsed device. One possible observation that can be made here is that calculations for an oscillator operating high above threshold produce population distributions which do not extend appreciably above $v \geq 15 - 20$ (since stimulated emission rates compete favorably with kinetic rates and prevent highly populated upper levels). Thus, for these cases, a (possibly) incorrect theory for rates in the highest v -levels would not affect the results. The theoretical understanding of the VVT cross-relaxation rates is still an open and controversial question, and will require substantial future effort to resolve conclusively. Some of the experimental measurements that are being carried out to obtain a better VV rate matrix are described below, and the comparisons of the calculations with the E-beam laser results are discussed in Section 3.0.

2.3 Rate Constant Measurements. (U) An accurate knowledge of the rate of energy exchange between various vibrational levels of the CO molecule is essential for a successful computer code to predict the characteristics of the CO laser. However, obtaining

UNCLASSIFIED

such knowledge has proved to be a rather difficult task. This is mostly because of the large number of vibrational energy levels involved, which have greatly differing extent of coupling between them. So far, no single theory has been able to predict satisfactorily all of the 1600 rates which would be encountered if 40 levels are considered. Any experimental rate measurement is complicated by the fact that one invariably measures a quantity which is intimately related to the relaxation of the whole ensemble of levels, rather than any particular level, and therefore has to be interpreted in terms of a kinetic model.

(U) In view of the above difficulties two types of experimental measurements were selected after careful consideration of various alternatives. The two types of measurement are: (1) small signal gain measurements under steady state conditions for as many vibrational transitions as possible, and (2) transient gain measurement for a particular vibrational-rotational transition following saturation of a transition between another pair of levels. Both of these experiments offer the advantage of carefully bringing the ensemble of CO vibrational levels to an equilibrium and perturbing only one particular transition at a time. Therefore, this scheme eliminates the uncertainties involved in previously employed methods such as Q-switching, pulsed electrical excitation¹⁸ and deactivation by foreign molecules.¹⁷ The details of the present investigation are described below.

Small Signal Gain Measurements. (U) The most direct as well as accurate determination of the population densities of the various vibrational levels is obtained from the measurement and analysis of the small signal gains. The

UNCLASSIFIED

population density distribution for a large number of levels under steady state conditions is one of the key measurements that can be used to verify accuracy of the rate matrix for vibrational energy exchange. This is, of course, possible because of the fact that a reasonably accurate value is available for the other parameters used in the modeling, viz., the electron and molecular densities, electron and molecular temperatures, electron excitation cross sections, etc. The only other uncertainty is the VT rates for the higher vibrational levels. Since these rates are small to begin with, the inaccuracy in the assumed VT rates probably would not seriously affect the results of the kinetic modeling.

(U) The details of the experimental arrangement for the gain measurement have been described previously.¹³ The analytical procedure for determining the population density distribution from the experimental gain data was also described there. In the present investigation, a mixture containing only CO, He and O₂ was used, and a large number of vibrational bands from $v = 4$ to $v = 24$ were covered. The measured gains and the resulting population densities for CO concentrations of 0.1, 0.2, 0.3 and 0.4 torr are given in Table 2.1 and 2.2, and a semilog plot of the population densities is given in Figure 2.2.

(U) The theoretical population densities for a CO concentration of 0.3 torr obtained by kinetic modeling are shown in Figure 2.3. The VV rate matrix used in these calculations is that given by Jeffers and Kelley. It is evident from the figure that unusually large population densities at higher V-bands are predicted theoretically if the probabilities used for the rate matrix are not truncated at some arbitrary value. The inadequacy of the

UNCLASSIFIED

(U) Table 2.1. Small Signal Gain for Various Vibrational Rotational Transitions of CO. (U)

Branch v → v-1	J	G Out/In	Meas. Gain Pct/cm
Partial Pressure of CO = 0.1 torr			
7 - 6	15	1.27	.193
8 - 7	9	1.90	.539
	10	1.91	.522
	12	1.64	.399
	14	1.38	.260
9 - 8	8	1.24	.174
10 - 9	13	1.48	.316
	12	1.61	.384
	10	1.80	.474
	11	1.78	.465
11-10	8	1.76	.456
	9	1.84	.492
	10	1.90	.518
	11	1.68	.418
	12	1.57	.364
	13	1.49	.322
12 - 11	8	2.02	.567
	9	1.98	.551
	10	1.84	.492
	14	1.35	.242
13 - 12	9	1.77	.461
	13	1.43	.288
	10	1.72	.437
	12	1.50	.327
	11	1.73	.442
14 - 13	7	1.63	.394
	8	1.68	.418
	11	1.61	.384
	13	1.44	.294
15 - 14	10	1.59	.374
	14	1.25	.180
	11	1.62	.389

UNCLASSIFIED

(U) Table 2.1. Small Signal Gain for Various Vibrational Rotational Transitions of CO (continued). (U)

Branch v → v-1	J	G Out/In	Meas. Gain Pct/cm
Partial Pressure of CO = 0.1 torr			
16 - 15	12	1.44	.294
	9	1.57	.364
17 - 16	11	1.40	.271
18 - 17	11	1.40	.271
	12	1.36	.248
	9	1.41	.277
19 - 18	8	1.50	.327
	9	1.53	.343
	10	1.51	.332
	11	1.40	.271
20 - 19	12	1.25	.180
21 - 20	9	1.29	.205
22 - 21	7	1.17	.127
	10	1.26	.186
23 - 22	10	1.19	.140
24 - 23	8	1.14	.106
	11	1.20	.147
Partial Pressure of CO = 0.2 torr			
7 - 6	15	1.34	.236
8 - 7	9	2.23	.647
	10	2.08	.591
	12	1.36	.501
	14	1.53	.343

UNCLASSIFIED

(U) Table 2.1. Small Signal Gain for Various Vibrational Rotational Transitions of CO (continued). (U)

Branch v → v-1	J	G Out/In	Meas. Gain Pct/cm
Partial Pressure of CO = 0.2 torr			
9 - 8	9	1.90	.518
	13	1.71	.433
10 - 9	8	2.26	.658
	9	2.29	.669
	10	2.24	.650
	11	2.24	.650
	12	1.93	.530
	13	1.71	.433
11 - 10	8	2.23	.647
	9	2.16	.621
	10	2.36	.693
	11	2.06	.583
	12	1.91	.522
	13	1.74	.447
12 - 11	8	2.26	.789
	9	2.50	.739
	10	2.29	.669
	10	2.17	.625
	11	2.01	.563
	12	1.80	.474
	13	1.69	.423
	14	1.53	.343
13 - 12	9	2.06	.583
	10	2.19	.632
	11	2.19	.632
	12	1.76	.456
	13	1.63	.394
14 - 13	7	2.05	.579
	8	2.08	.591
	10	2.53	.749
	11	2.03	.571
	13	1.69	.423
	14	1.58	.369

UNCLASSIFIED

(U) Table 2.1. Small Signal Gain for Various Vibrational Rotational Transitions of CO (continued). (U)

Branch $v \rightarrow v-1$	J	G Out/In	Meas. Gain Pct/cm
Partial Pressure of CO = 0.2 torr			
15 - 14	10	2.02	.567
	11	2.05	.579
	12	1.60	.379
	13	1.60	.379
	14	1.46	.305
16 - 15	9	1.96	.543
	12	1.70	.428
	13	1.51	.332
17 - 16	10	1.90	.518
	11	1.68	.418
	12	1.55	.353
18 - 17	9	1.69	.423
	11	1.66	.409
	12	1.74	.448
	12	1.58	.369
19 - 18	8	1.89	.513
	9	1.90	.518
	10	1.81	.479
	11	1.68	.418
20 - 19	12	1.39	.266
21 - 20	7	1.44	.294
	8	1.47	.310
	9	1.52	.338
	10	1.41	.277
	11	1.43	.288
22 - 21	7	1.31	.218
	7	1.29	.205
	8	1.51	.332
	9	1.32	.224
	10	1.50	.327

UNCLASSIFIED

(U) Table 2.1. Small Signal Gain for Various Vibrational Rotational Transitions of CO (continued). (U)

Branch v → v-1	J	G Out/In	Meas. Gain Pct/cm
Partial Pressure of CO = 0.2 torr			
23 - 22	10	1.35	.242
22 - 21	11	1.39	.266
	12	1.48	.316
24 - 23	8	1.24	.174
	11	1.32	.224
Partial Pressure of CO = 0.3 torr			
7 - 6	15	1.40	.271
8 - 7	9	2.36	.693
	10	2.21	.640
	12	1.98	.551
	14	1.62	.389
9 - 8	9	1.91	.522
	13	1.83	.487
10 - 9	8	2.48	.733
	9	2.51	.742
	10	2.58	.764
	11	2.66	.790
	12	2.16	.621
	13	1.86	.501
11 - 10	8	2.47	.729
	9	2.39	.703
	10	2.72	.807
	11	2.35	.689
	12	2.17	.625
	13	1.92	.526
12 - 11	9	2.93	.867
	10	2.66	.789
	13	1.84	.492
	14	1.66	.409

UNCLASSIFIED

(U) Table 2.1. Small Signal Gain for Various Vibrational Rotational Transitions of CO (continued). (U)

Branch $v \rightarrow v-1$	J	G Out/In	Meas. Gain Pct/cm
Partial Pressure of CO = 0.3 torr			
13 - 12	11	2.50	.739
	13	1.78	.465
14 - 13	8	2.33	.682
	10	2.70	.801
	11	2.31	.675
	13	1.85	.496
15 - 14	10	2.29	.668
	11	2.32	.679
	13	1.82	.483
	14	1.61	.384
16 - 15	?	2.16	.621
	12	1.93	.530
	13	1.69	.423
17 - 16	10	2.25	.654
	10	2.06	.583
	11	1.92	.526
	12	1.74	.447
18 - 17	11	1.89	.513
	9	1.96	.543
	12	1.76	.456
19 - 18	9	2.23	.647
	10	2.08	.591
	11	1.89	.513
20 - 19	12	1.51	.332
21 - 20	7	1.58	.369
	8	1.60	.379
	9	1.69	.423
	10	1.56	.359
	11	1.54	.348

UNCLASSIFIED

(U) Table 2.1. Small Signal Gain for Various Vibrational Rotational Transitions of CO (continued). (U)

Branch v → v-1	J	G Out/In	Meas. Gain Pct/cm
Partial Pressure of CO = 0.3 torr			
22 - 21	7	1.40	.271
	7	1.42	.283
	8	1.68	.418
	9	1.44	.294
	10	1.68	.418
	11	1.55	.353
	11	1.56	.359
	12	1.64	.399
	12	1.65	.404
23 - 22	10	1.49	.322
24 - 23	8	1.33	.227
	11	1.40	.271
15 - 14	12	1.86	.501
13 - 12	12	2.54	.752
	12	1.92	.526
	9	2.23	.647
12 - 11	12	2.00	.560
	11	2.25	.654
	8	3.16	.928
9 - 8	13	1.85	.496
Partial Pressure of CO = 0.4 torr			
7 - 6	15	1.44	.294
8 - 7	9	2.38	.699
	10	2.25	.654
	12	2.06	.583
	14	1.69	.423

UNCLASSIFIED

(U) Table 2.1. Small Signal Gain for Various Vibrational Rotational Transitions of CO (continued). (U)

Branch $v \rightarrow v-1$	J	G Out/In	Meas. Gain Pct/cm
Partial Pressure of CO = 0.4 torr			
9 - 8	9	1.88	.509
	13	1.93	.530
10 - 9	10	2.82	.836
	11	3.10	.912
	9	2.70	.801
11 - 10	9	2.52	.745
	11	2.60	.771
12 - 11	10	2.80	.830
	11	2.45	.723
	12	2.14	.614
	13	1.96	.543
	14	1.77	.461
	12	2.18	.629
	11	2.48	.733
	11	2.71	.804
	13	2.01	.563
13 - 12	13	1.93	.530
	9	2.34	.686
	11	2.71	.304
	12	2.03	.571
	13	2.78	.825
14 - 13	8	2.48	.733
	7	2.55	.755
	14	1.84	.492
	13	1.96	.543
	11	2.49	.736
	10	3.05	.899
15 - 14	10	2.46	.726
	11	2.51	.742
	12	2.08	.591
	13	1.80	.474
	14	1.72	.437
16 - 15	9	2.31	.675
	12	2.09	.595
	13	1.84	.492

UNCLASSIFIED

(U) Table 2.1. Small Signal Gain for Various Vibrational Rotational Transitions of CO (continued). (U)

Branch v → v-1	J	G Out/In	Meas. Gain Pct/cm
Partial Pressure of CO = 0.4 torr			
17 - 16	10	2.18	.629
	11	2.10	.598
	12	1.91	.522
18 - 17	9	2.14	.614
	11	2.08	.591
	11	2.10	.598
	11	2.09	.595
	12	0.85	.496
	12	2.03	.571
	12	1.89	.513
	13	1.55	.353
19 - 18	8	2.18	.629
	11	2.03	.571
	10	2.31	.675
	9	2.44	.719
	8	2.21	.640
20 - 19	12	1.58	.369
21 - 20	7	1.69	.423
	8	1.69	.423
	9	1.84	.492
	10	1.67	.414
	11	1.63	.394
22 - 21	8	1.78	.465
	9	1.50	.327
	10	1.80	.474
	7	1.51	.332
	7	1.47	.311
	11	1.71	.433
	12	1.77	.461
23 - 22	10	1.60	.379
24 - 23	8	1.40	.271
	11	1.48	.316

UNCLASSIFIED

(U) Table 2.2. CO Population Densities as Derived from Gain Measurements. (U)

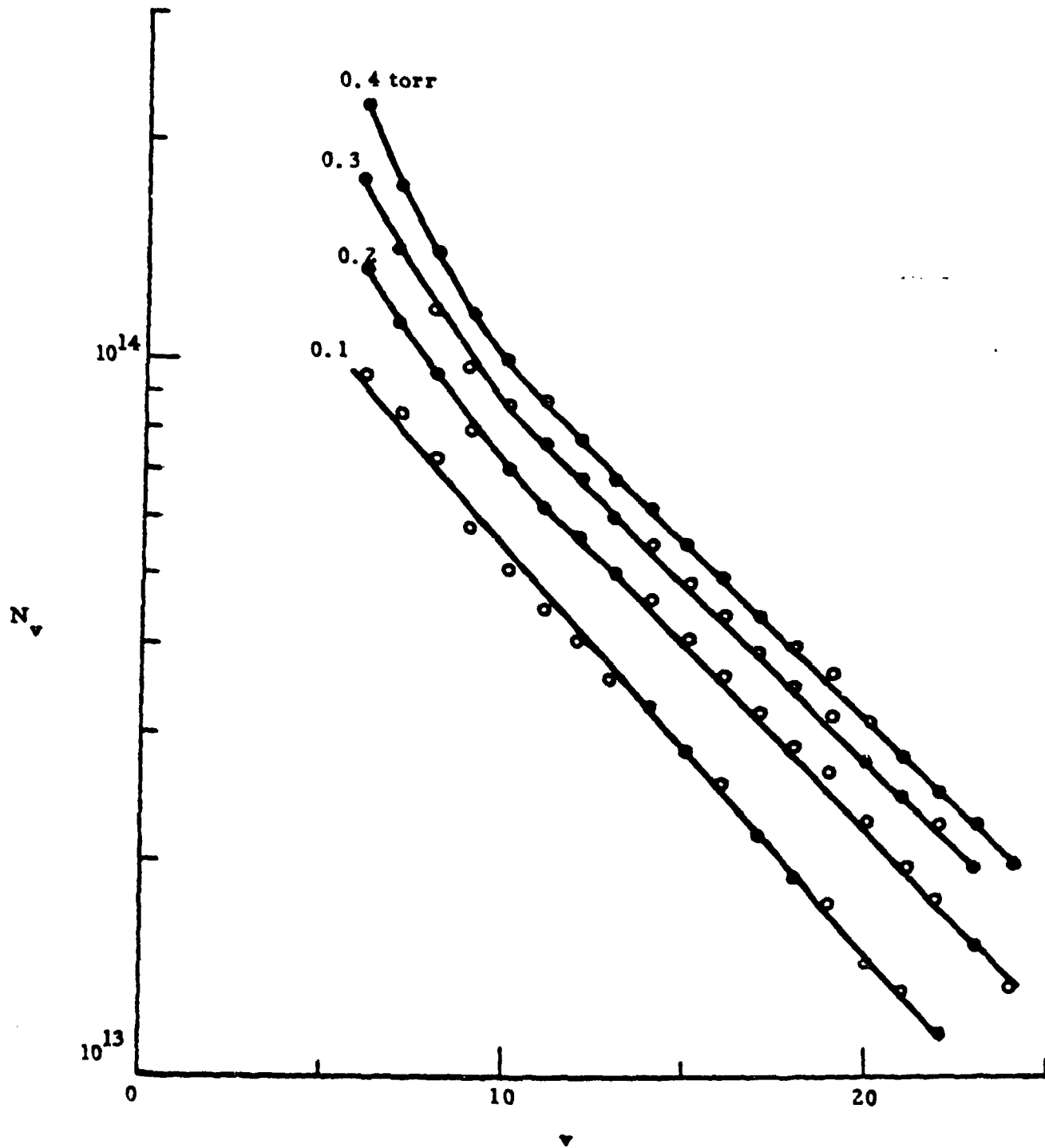
$T_{\text{mol}} = 150^{\circ}\text{K}$ $P(\text{CO}) = .10 \text{ torr}$ $P(\text{He}) = 10.00 \text{ torr}$	$N_{\nu} \times 10^{-13} (\text{cm}^{-3})$	$T_{\text{mol}} = 152^{\circ}\text{K}$ $P(\text{CO}) = .20 \text{ torr}$ $P(\text{He}) = 10.00 \text{ torr}$	$N_{\nu} \times 10^{-13} (\text{cm}^{-3})$
ν		ν	
6	9.456	6	13.25
7	8.413	7	11.19
8	7.236	8	9.488
9	5.771	9	7.965
10	5.082	10	7.021
11	4.492	11	6.213
12	4.088	12	5.612
13	3.623	13	4.992
14	3.244	14	4.552
15	2.865	15	4.062
16	2.532	16	3.622
17	2.177	17	3.207
18	1.910	18	2.857
19	1.749	19	2.632
20	1.489	20	2.222
21	1.304	21	1.978
22	1.143	22	1.760
23	0.974	23	1.530
24	0.847	24	1.337

UNCLASSIFIED

(U) Table 2.2. CO Population Densities as Derived from Gain Measurements. (continued). (U)

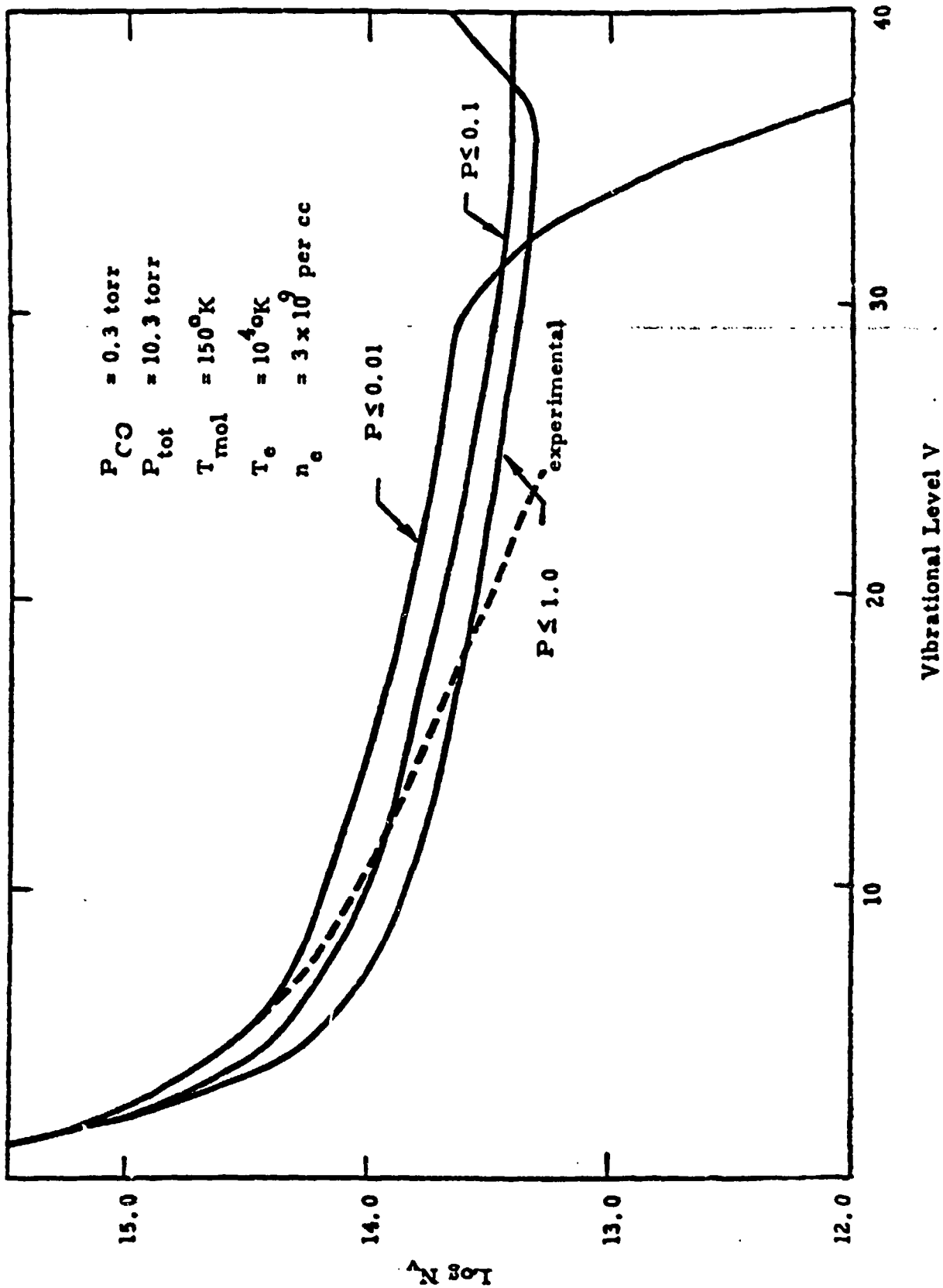
T _{mol} P(CO) P(H ₂)	155°K = .30 torr = 10.00 torr	T _{mol} P(CO) P(H ₂)	= 159°K = .40 torr = 10.00 torr
v	N _v x 10 ⁻¹³ (cm ⁻³)	v	N _v x 10 ⁻¹³ (cm ⁻³)
6	17.75	6	22.40
7	14.27	7	17.28
8	11.86	8	14.14
9	9.807	9	11.52
10	8.581	10	10.07
11	7.553	11	8.685
12	6.829	12	7.646
13	6.071	13	6.754
14	5.481	14	6.150
15	4.915	15	5.507
16	4.383	16	4.925
17	3.921	17	4.381
18	3.502	18	3.943
19	3.230	19	3.649
20	2.751	20	3.107
21	2.462	21	2.800
22	2.213	22	2.531
23	1.948	23	2.250
24	1.708	24	1.990

UNCLASSIFIED



(U) Figure 2.2. Population densities of the various vibrational levels at different CO partial pressures as derived from gain measurements. (U)

UNCLASSIFIED



(U) Figure 2.3. Effect of probability truncation on population distribution. (U)

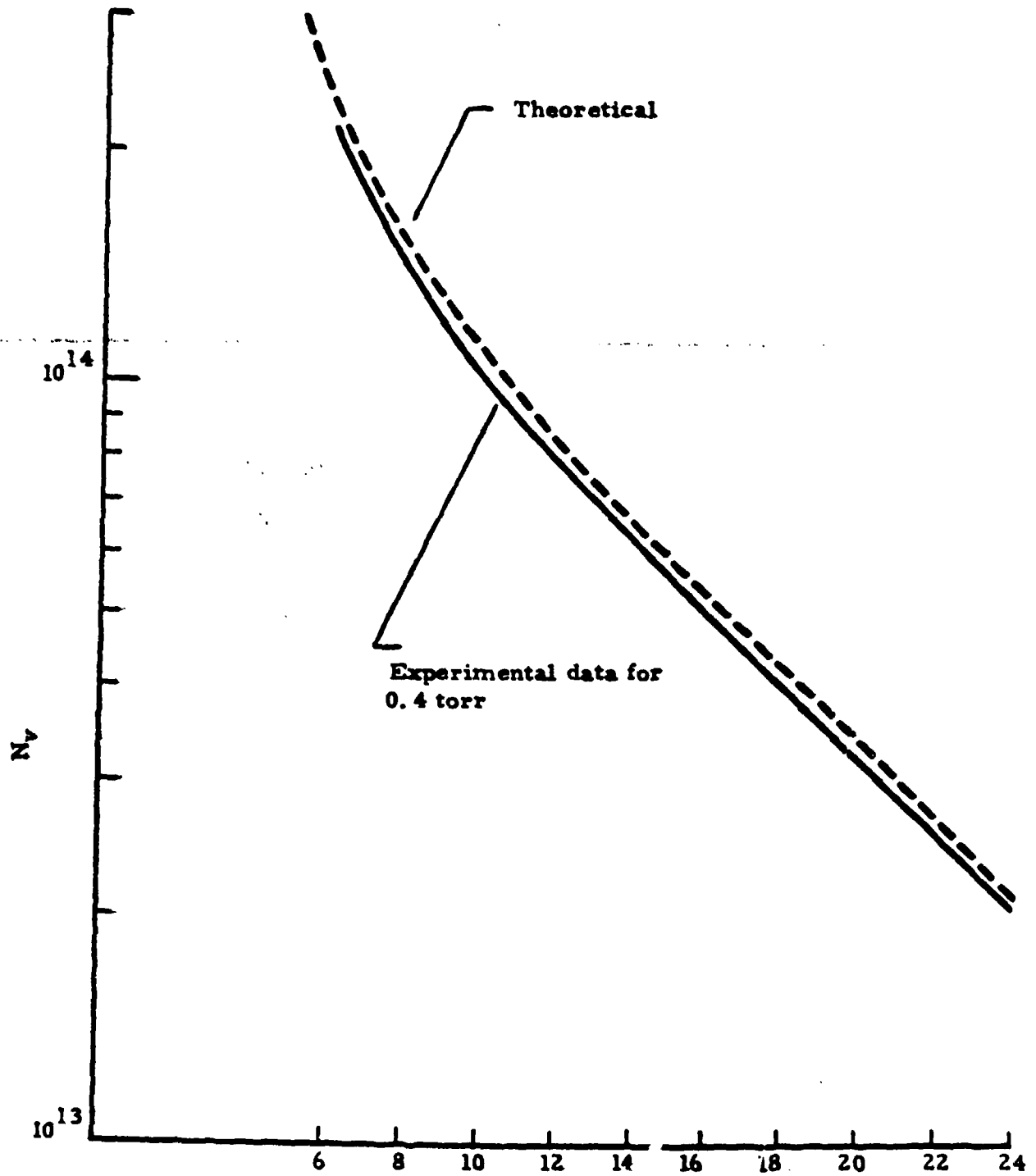
UNCLASSIFIED

Jeffers and Kelley theory (considered to be the best so far) is evident. Under the circumstances, a preliminary approximation has been to construct a "phenomenological" matrix obtained by truncating the probability at a proper value so that the rate matrix is able to predict the observed population density. The dotted curve in Figure 2.3 gives the experimentally measured population densities. Comparison of the experimental and theoretical curves show that a reasonable value for probabilities truncation is ~ 0.01 . Attempts are continuing for modifying the rate matrix for a better fit of the theoretical population densities to the experimental data, especially with those obtained with other CO concentrations.

(U) It is interesting to note that if the probabilities in the Jeffers and Kelley theory are truncated at ~ 0.01 , the resultant rate matrix begins to resemble that obtained from the SSH theory except for some differences in only a few rates (out of the total of 1600). This apparently minor difference in the rates seems to make a significant impact on the modeling of the transient phenomena such as the measurements of gain variation described below. This is probably due to the fact that resonant near neighbors play a dominant role in transient experiments. However, since the majority of the rates in the SSH theory are similar to those in the modified Jeffers and Kelley theory, the former may also be used for modeling steady state conditions. This is illustrated in Figure 2.4, where the experimental population distribution is seen to be close to that obtained by modeling using the SSH theory. Furthermore, a proper force fit of the SSH theory may be obtained to predict the transient measurements also. Therefore, it seems possible that a "phenomenological" matrix may be constructed by modification of either theory.

Transient Gain Measurements. (U) The measurement of the rate of change of gain following a saturating pulse has been one attempt made to

UNCLASSIFIED



(U) Figure 2.4. Comparison of experimentally measured population densities (given by solid curve) with those theoretically using SSH theory. (U

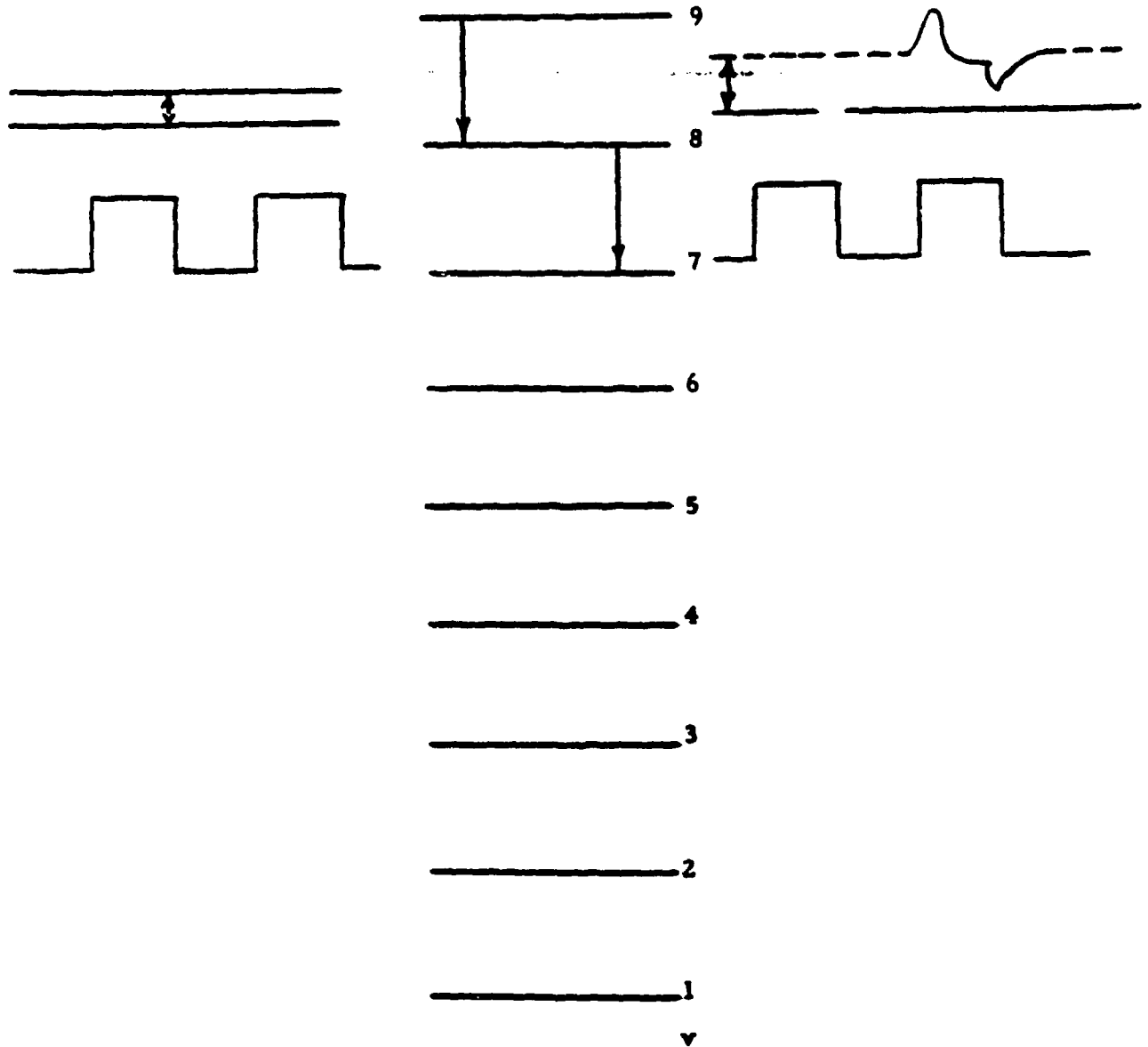
UNCLASSIFIED

UNCLASSIFIED

determine vibrational relaxation rates. The principle of the experiment is depicted in Figure 2.5 and 2.6. In this example, the small signal gain of a transition between $v = 9$ to $v = 8$ is monitored by means of a probe beam of low intensity ($\sim 1 \text{ mW/cm}^2$), while simultaneously, a spatially congruent chopped, high intensity beam ($\sim 1 \text{ W/cm}^2$) is allowed to saturate the amplifier on a transition between $v = 8$ to $v = 7$. In order to increase sensitivity, the detector is ac-coupled so that only the changes in the gain are recorded. As soon as the saturating pulse between 8-7 is turned on, the gain between 9-8 increases because of the sudden depopulation of the level $v = 8$ by stimulated emission. Due to VV relaxation, the population of the level $v = 8$ gradually comes to an equilibrium close to its former value, even though the saturating pulse is kept turned on. The resulting decay curve for the gain of the 9-8 transition contains the VV rate information. When the saturating pulse is finally turned off, exactly the opposite happens. Either of the decay curves may be utilized for extracting the VV rate information.

(U) The experimental arrangement is schematically shown in Figure 2.6. The probe and the saturating laser lines are selected by the gratings in the respective optical cavity. The two beams are then made congruent by means of a 50% beam splitter. Before reaching the beam splitter, the intensity of the probe beam was actually increased by a factor of ~ 3 by means of a telescope. A chopper was placed at the focal plane of the telescope for a fast pulse turn on. The two beams, after passing through the steady state amplifier, were separated by a SPEX monochromator provided with an InSb detector. The signal to noise ratio of the detector output was greatly increased by employing a synchronous detection scheme using a PAR Model M-160 boxcar integrator. The discharge in the laser and the optical amplifier were stabilized by electronic current controllers. The various transitions studied are listed in Table 2.3.

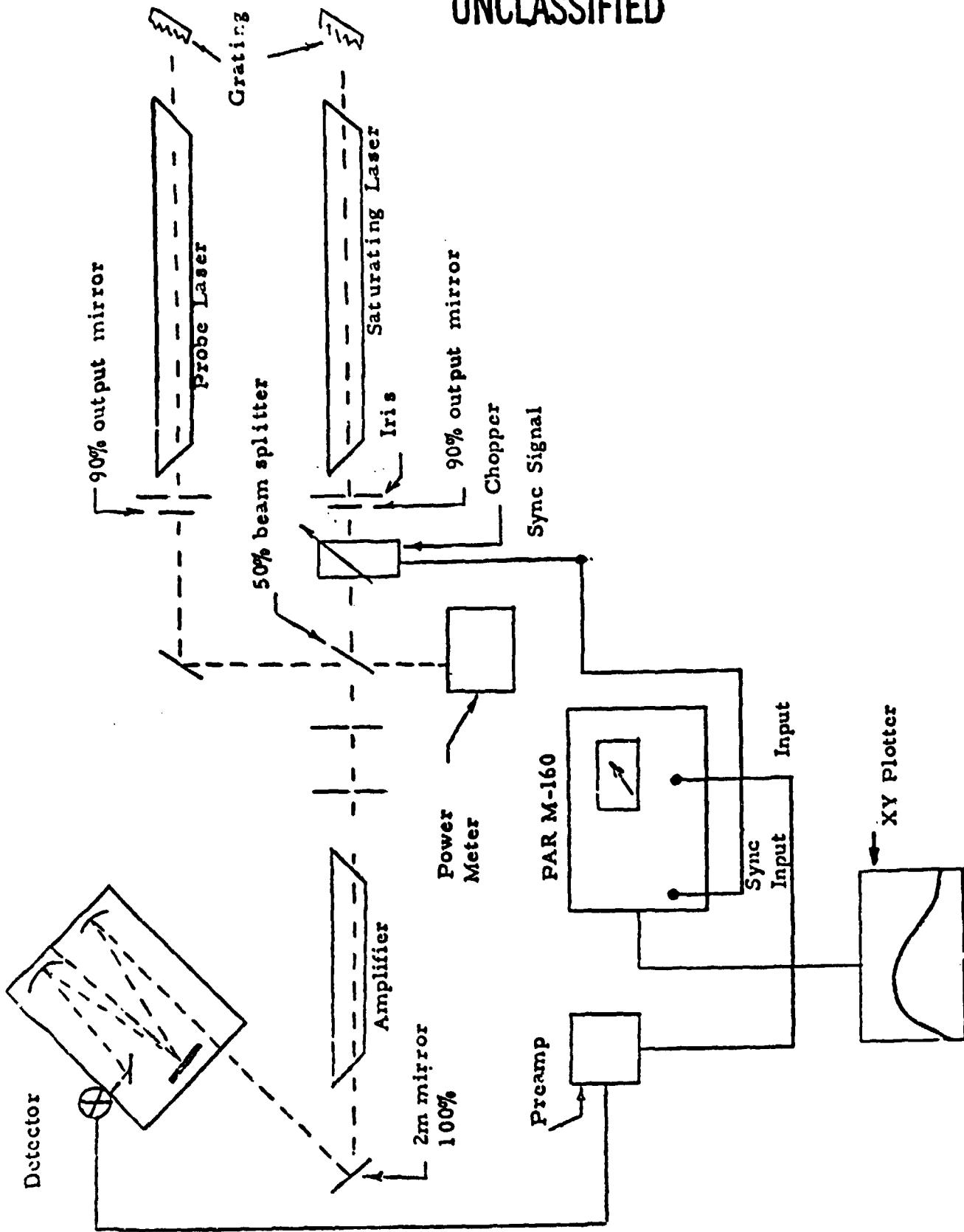
UNCLASSIFIED



(U) Figure 2.5. Relaxation measurement scheme. (U)

UNCLASSIFIED

UNCLASSIFIED



(U) Figure 2.6. Experimental arrangement for relaxation measurement. (U)

UNCLASSIFIED

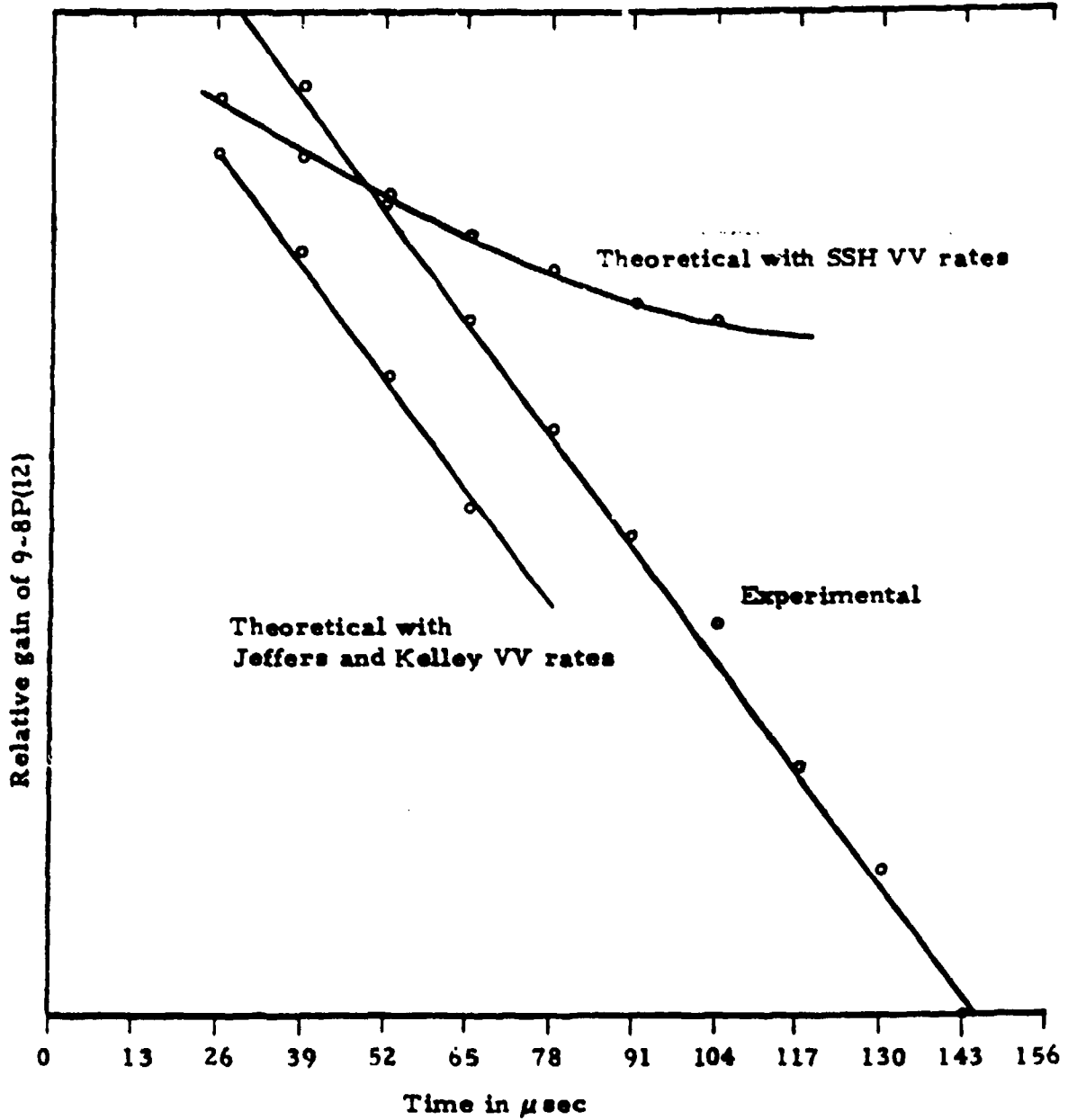
UNCLASSIFIED

(U) Table 2.3. Summary of VV Relaxation Studies. (U)

<u>Probe Line</u>	<u>Saturation Line</u>	<u>Saturating Intensity W/cm²</u>	<u>CO Partial Pressure torr</u>
7-6P(11)	8-7P(12)	1.2	.65
8-7P(12)	9-8P(13)	1.5	.59
9-8P(12)	8-7P(12)	2.5	.99
9-8P(12)	8-7P(12)		.54
10-9P(10)	9-8P(13)	1.4	.48

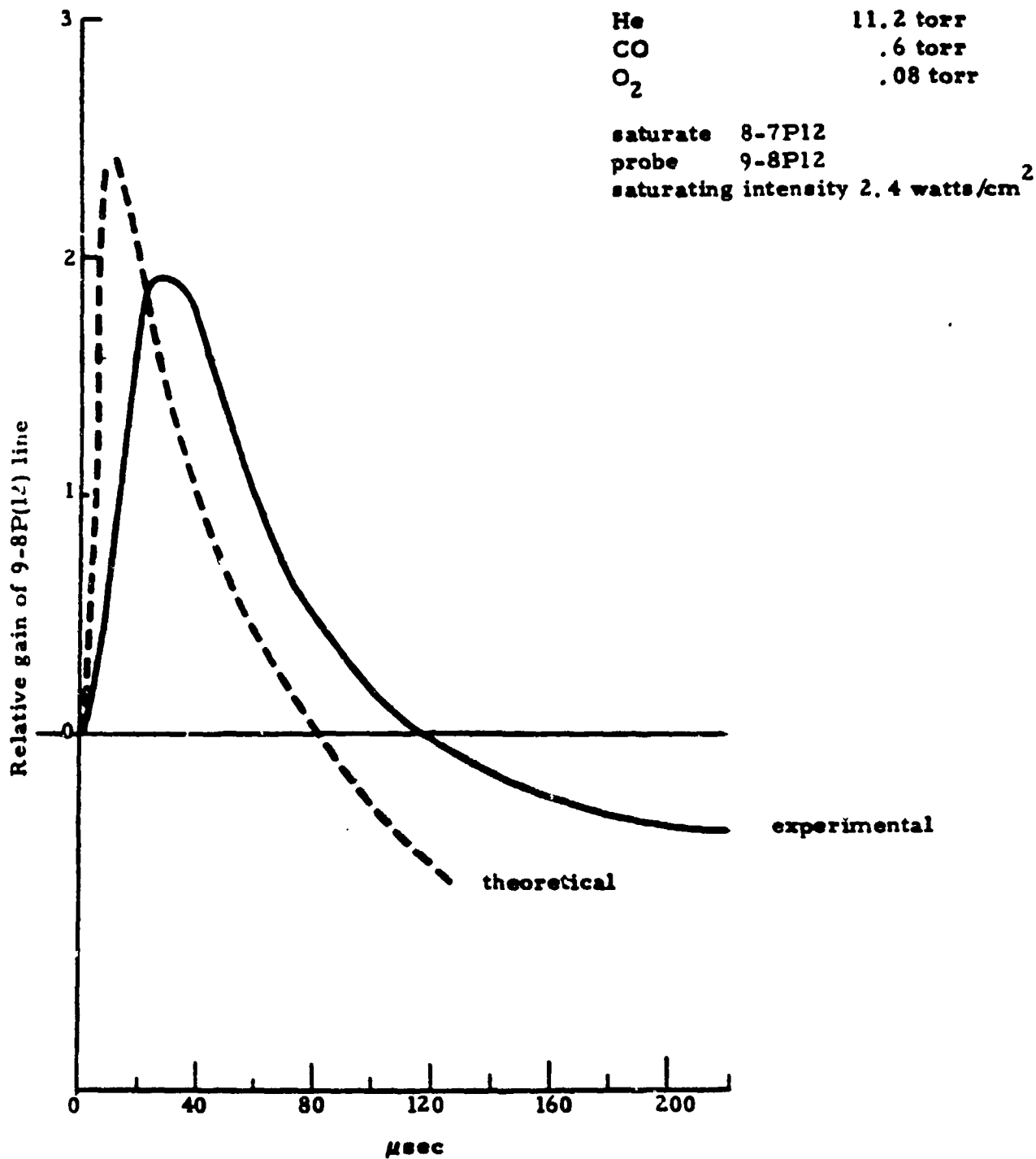
(U) Figure 2.7 shows a typical decay curve. In this case the probe laser was operated on the 9-8P(12) line while the saturating laser was tuned to the 8-7P(12) line. The dotted line in Figure 2.7 shows the gain decay curve obtained by modeling. The slow turn on time in the experimental curve is mainly due to an insufficient chopper speed, although it could be attributed partly to insufficient bandwidth of the preamplifiers. The difference between the two curves at longer times seems to be primarily due to insufficient bandwidth. The results are now being repeated with a larger bandwidth preamplifier. Also a more accurate determination of the CO concentration by means of a residual gas analyzer is in progress.

(U) The inadequacy of the SSH theory in explaining transient measurement is vividly demonstrated in Figure 2.8. Using a semilog plot of the curve in this figure it is evident that the slope of the theoretically obtained line using Jeffers and Kelley theory resembles that of the experimental line while that obtained by using SSH theory is quite different.



(U) Figure 2. 8. Time variation of gain of 9-8P(12) line in presence of a 8-7P(12) saturation pulse of $2.4\text{W}/\text{cm}^2$.

UNCLASSIFIED



(U) Figure 2.7. Time variation of gain in presence of a saturation pulse. (U)

UNCLASSIFIED

(U) At this stage of the investigation neither the Jeffers and Kelley nor the SSH theory are able to predict the critical VV rates required for our theoretical model. Modifications of either theory are necessary to explain experimental results obtained under carefully controlled conditions.

UNCLASSIFIED

3.0 E-BEAM STABILIZED DISCHARGE LASER RESULTS

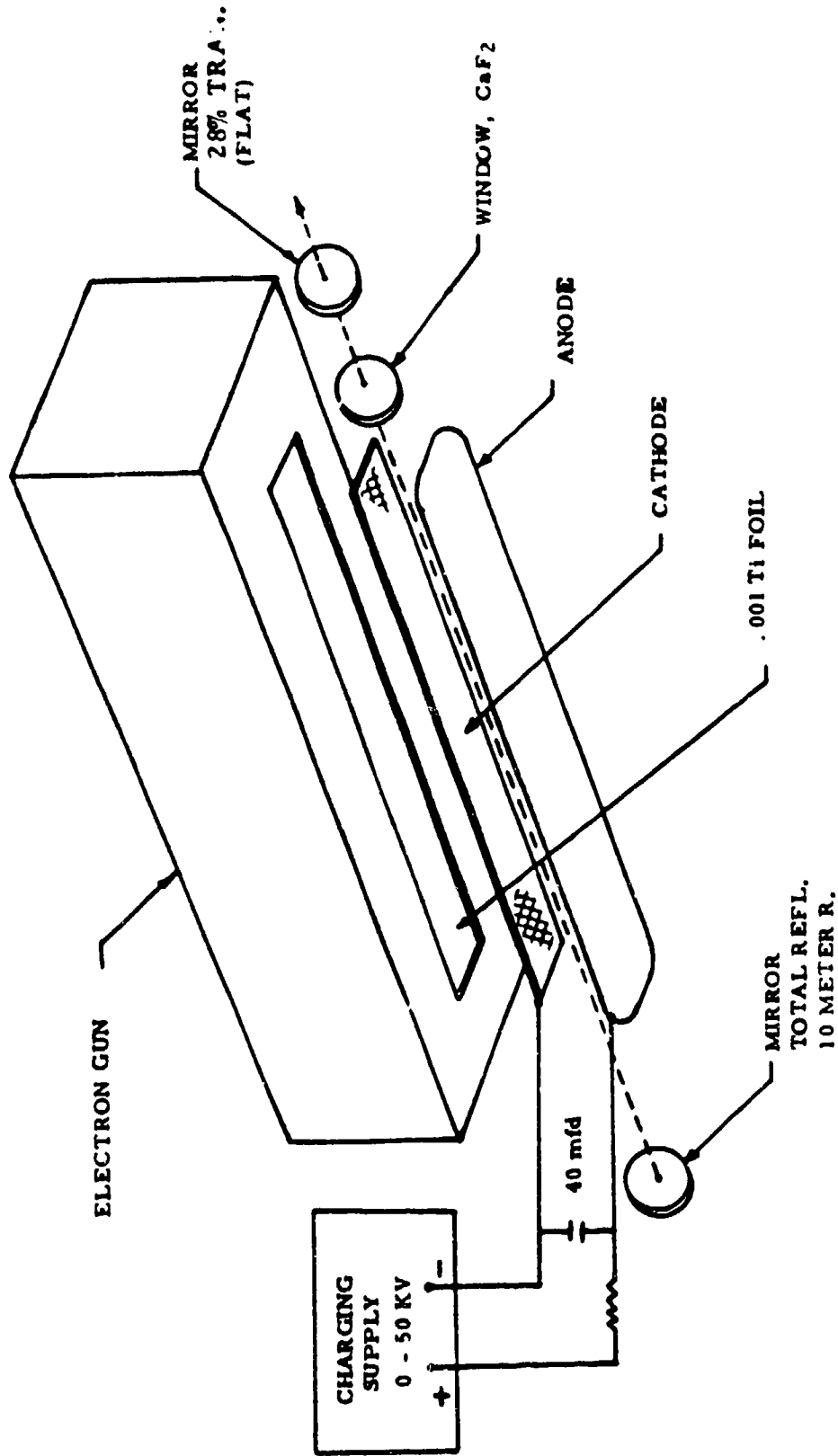
(U) An E-beam stabilized electrical discharge CO laser has been operated under a variety of experimental conditions. The experimental configuration is described in Section 3.1 below, followed by a discussion in 3.2 of some of the results obtained to date.

3.1 Experimental Description. (U) The experimental E-beam device is shown pictorially in Figure 3.1 and in schematic cross section in Figure 3.2. The discharge volume is approximately 5 x 5 x 100 cm. Precooled gas flows through the anode which includes a heat exchanger with provision for liquid nitrogen cooling. The gas passes out of the anode through a sintered porous screen on the anode surface, flows across the discharge volume as indicated in Figure 3.2, and is extracted by two thin manifolds which extend the length of the discharge region between the sustainer cathode and the gun. The sides of the discharge region are enclosed by foam insulated Lexan walls.

(U) The ends of the active volume are thermally isolated from ambient by evacuated cells. At the output end, two AR coated CaF_2 windows are employed with the output coupling mirror (hole coupled or unstable optics) disposed between them. The cell at the other end is formed by a single window and a total reflector. Gate valves at both ends permit the optics to be changed while the laser chamber is cold. The optics currently being used limit the active volume to less than 1 liter.

(U) The flow conditioning system is schematically represented in Figure 3.3. The gas flow and mixture are controlled by two stage dome

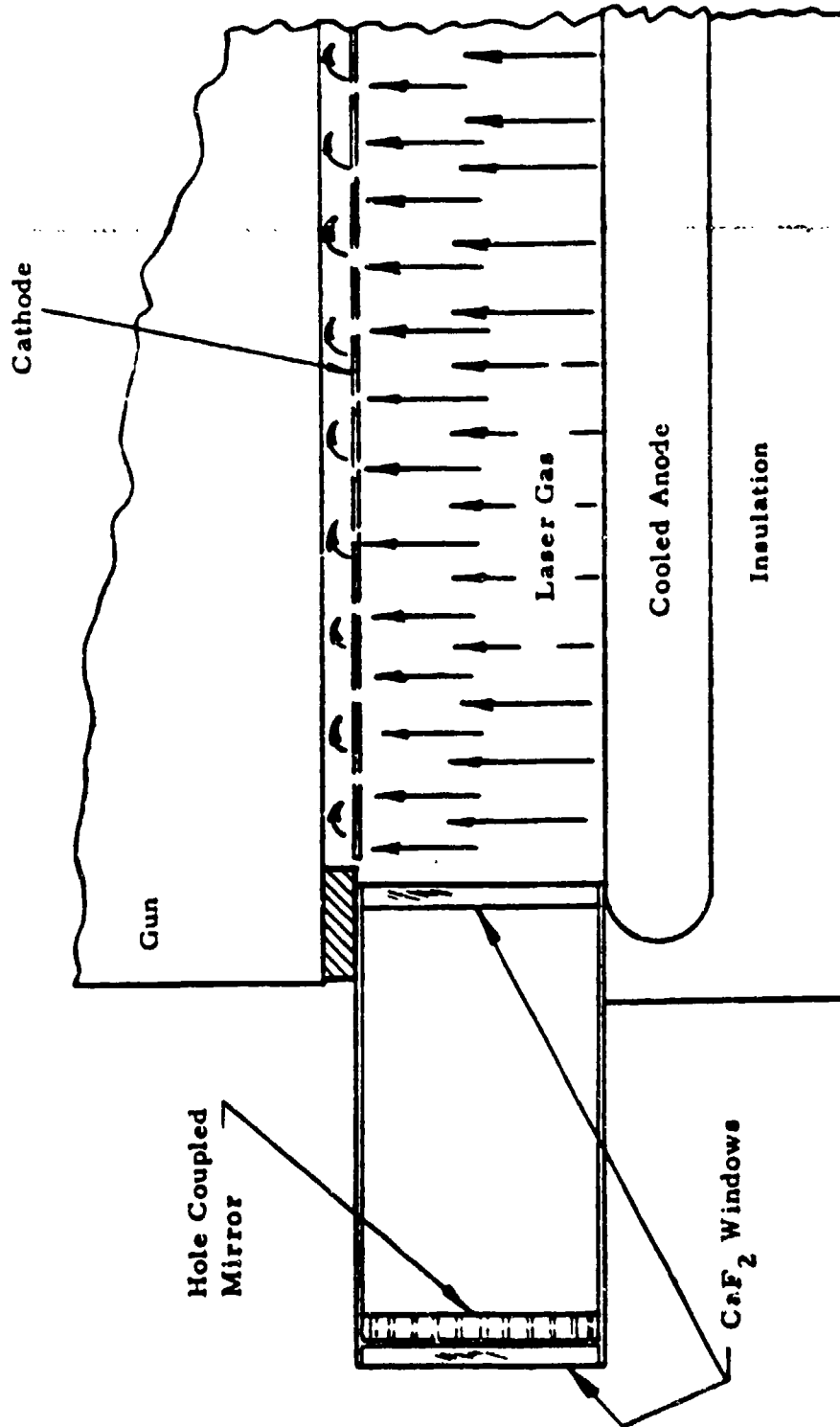
UNCLASSIFIED



(U) Figure 3.1. Experimental E-Beam Laser Configuration. (U)

UNCLASSIFIED

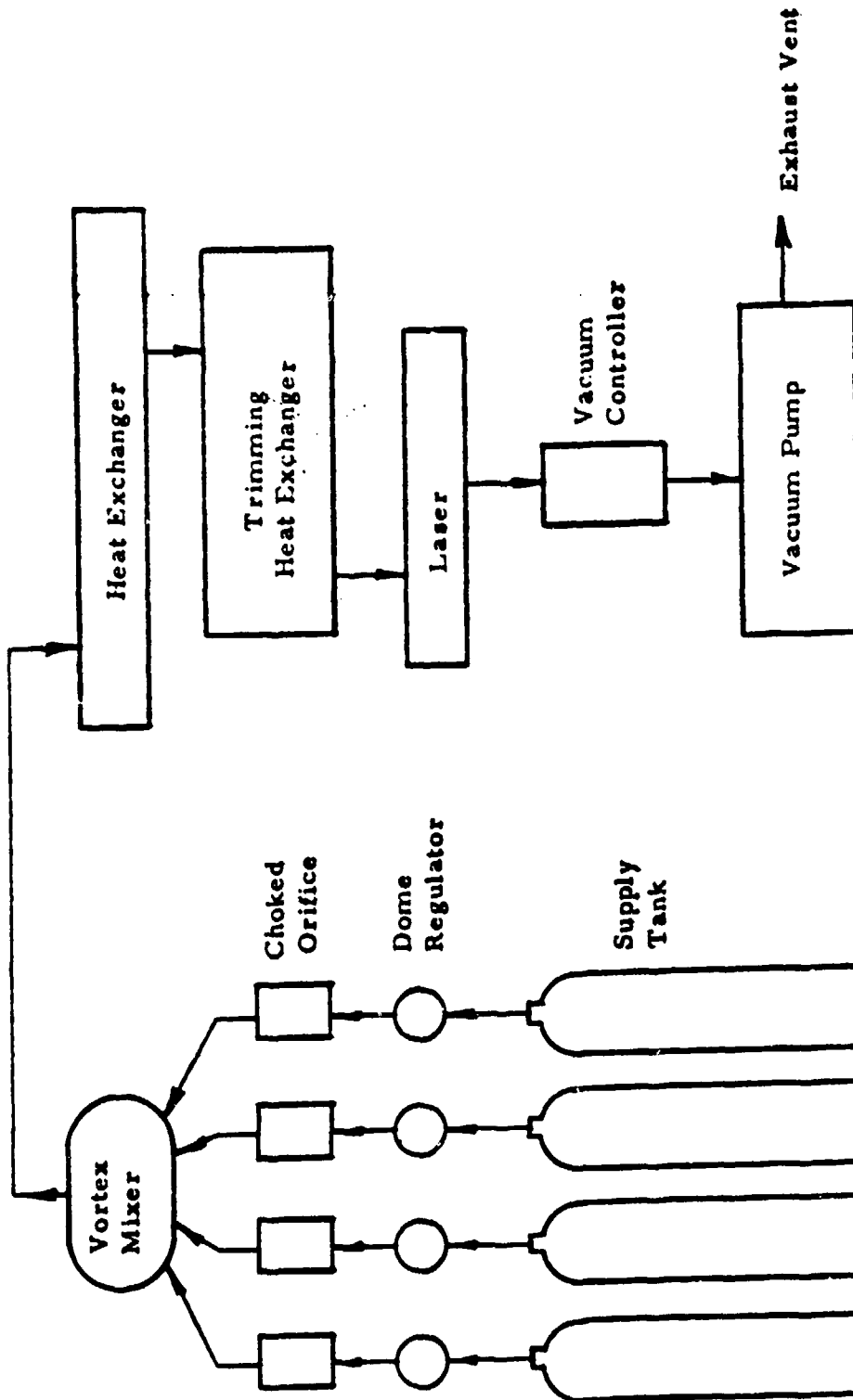
UNCLASSIFIED



(U) Figure 3.2. Flow System (U)

UNCLASSIFIED

UNCLASSIFIED



(U) Figure 3.3. Flow diagram for laser gas handling system. (U)

UNCLASSIFIED

UNCLASSIFIED

regulators and choked orifices. The gases are combined in a vortex mixer. A liquid nitrogen heat exchanger is employed for temperature conditioning. A trimming heat exchanger is currently being added to improve temperature control and uniformity. After passing through the laser, the gas is exhausted with a 300 CFM mechanical vacuum pump which is throttled by a vacuum controller which can maintain a preset pressure of 40 to 760 torr independent of flow rate.

(U) In most of the experiments performed to date, the gas temperature has been limited to a range above 150°K . At lower temperatures, difficulties were encountered with window seals and the gas distribution baffle in the anode. A modified assembly which should eliminate these deficiencies and permit operation down to 77°K is currently being completed.

(U) The electron gun used for the initial experiment discussed in the next section was built by Physics International. As delivered, the gun provided a beam current density of approximately 0.5 mA/cm^2 over an area of 3 cm x 100 cm with an accelerating voltage of approximately 165 kV. Considerable difficulty was encountered with vacuum integrity, excessive field emission, sparking, foil punctures, beam uniformity, and the modulator electronics. The performance and reliability of the gun were improved after it was converted from a triode to a tetrode configuration, the filament support system was improved, the vacuum envelope and foil support were extensively modified, and a new modulator was designed and constructed. After modification, it was possible to obtain approximately 3 mA/cm^2 over an output aperture of 5 cm x 100 cm with current density variations reduced to $\pm 20\%$.

(U) Construction of a Northrop designed gun has recently been completed and it has replaced the Physics International gun. In preliminary tests current densities in excess of 25 mA/cm^2 have been obtained with uniformity of $\pm 15\%$.

UNCLASSIFIED

(U) The sustainer is supplied from a capacitor bank which has an energy storage capability of 50 kJ at either 25 or 50 kV. The bank has an ignitron type crowbar which may be activated either in case of a fault or at a preset delay from the initiation of the gun pulse.

3.2 Experimental Results. (U) The E-beam stabilized electrical discharge CO laser has been operated over a range of electrical pumping rates for mixtures of CO and nitrogen and/or argon. Experiments have been carried out for pressures ranging from 50 torr to 760 torr and for temperatures ranging from 150°K to 300°K. Energy outputs of 28 J and peak powers greater than 500 kW have been obtained from an active volume slightly less than one liter. Electrical conversion efficiencies greater than 25% and specific energies greater than 100 J/liter-atm have also been obtained, with some of the experimental results summarized in Table 3.1. The first two cases correspond to an E-beam current density of 0.3 mA/cm² as obtained from the E-beam gun purchased from Physics International, Inc., modified by Northrop. The second case illustrates the improvement in output power, efficiency and specific energy by operating at cooled temperatures. Cases 3 and 4 correspond to a current density of 3.0 mA/cm² as obtained from the same E-gun modified by a Northrop designed pulsing unit. The improvements in output energy, specific energy and efficiency due to increased pumping is illustrated by case 3 and the results with a CO/Ar mix are illustrated in case 4. The brackets on the results for specific energies and efficiencies occur because of uncertainty in the active volume. The minimum values are based upon the active volume as defined by the system aperture, whereas the maximum values are defined by the active volume as estimated from measurements of the mode volume.

(U) Table 3.1. Typical E-Beam Experimental Results. (U)

I_B (ma/cr. ²)	INPUT LENGTH (μ s)	PULSE LENGTH (μ s)	PRESSURE (Torr)	MIXTURE	TEMPERATURE (°K)	OUTPUT (Joules)	SPECIFIC ENERGY (J/Liter - Atm)	EFFICIENCY (%)
0.3	300	300	760	CO:N2 1:2	300	1.9	5-6	1.2-1.5
0.3	230	230	200	CO:N2 1:1.5	150	11	40-80	5-10
3.0	110	110	200	CO:N2 1:4	150	26	100-200	12-24
3.0	85	85	200	CO:Ar 1:4	150	24	90-180	24-48

UNCLASSIFIED

UNCLASSIFIED

(U) Analytical results have indicated that the emitted spectrum shifts to lower vibrational bands as the electrical pumping rate is increased. This has been verified experimentally and the results for pumping rates of 2 kW/cc and 4 kW/cc are summarized in Table 3.2. In this table the letters to the right of the line designations indicated the relative strength and the brackets indicate cascades that occurred. Although the examples illustrated are for different gas mixtures, similar results have been obtained for the same mixture.

(U) Temporal laser pulse shapes obtained from the analytical model have been compared with the observed shapes and an example is shown in Figure 3.4. For this case the total pressure was 300 torr with gas composition of CO/Ar (1:4) at $\sim 150^{\circ}\text{K}$, and the electrical pumping rate was 6 kW/cc. The agreement with laser threshold time and the output peak power and energy are within a factor of two.

(U) As the electrical pumping rate is increased the peak power and efficiency increase and the threshold time decreases. The example illustrated in Figure 3.5 is 200 torr of CO/N₂ (1:3) with a peak electrical pump rate of approximately 2 kW/cc. In this case the laser output (top trace) does not begin until the sustainer current (bottom trace) shuts off. This strong after-pulse is typical of weakly pumped cases and is probably due to the inversion created when the direct electron-impact excitation to the lower vibrational levels is terminated at the end of the discharge. The long tail is also typical of mixtures using nitrogen and probably occurs because of the transfer of vibrational energy from nitrogen to CO.

(U) Two experimental examples with increased electrical pumping are illustrated in Figures 3.6 and 3.7. Figure 3.6 is again 200 torr of

UNCLASSIFIED

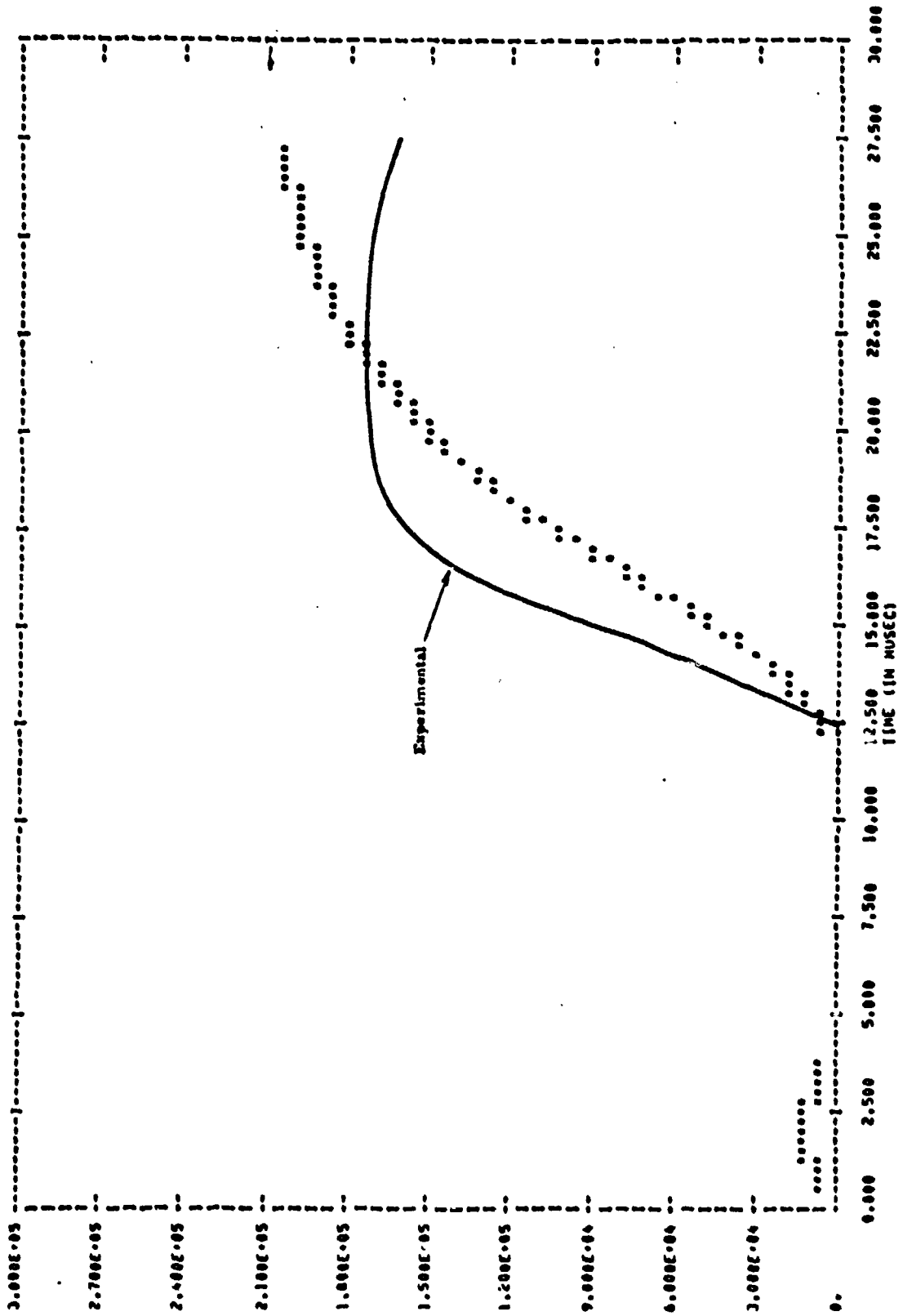
(U) Table 3.2. Typical Spectra. (U)

T = 150°K

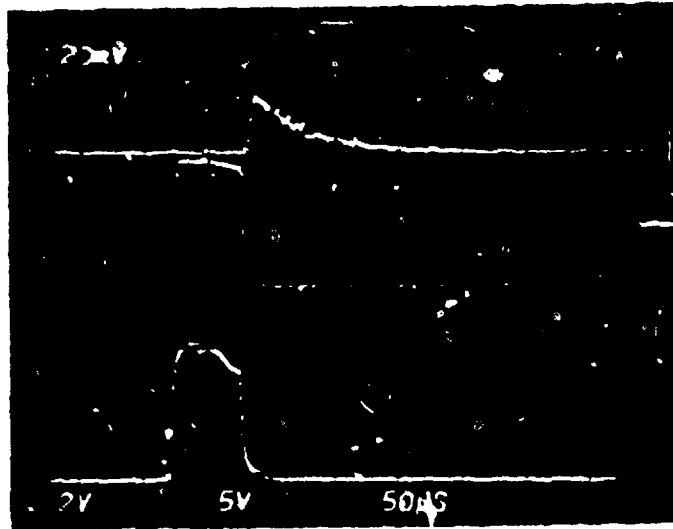
P = 300 Torr

MIXTURE	CO:Ar - 1:4	CO:N ₂ - 1:3
INPUT	4 kW/cm ³	2 kW/cm ³
PULSE DURATION	25 μs	200 μs
	<ul style="list-style-type: none"> 6-5 P(16) W 7-6 P(15) S 8-7 P(14) S 9-8 P(15) W 9-8 P(13) M 9-8 P(11) VW 10-9 P(15) VVW 10-9 P(14) W 	<ul style="list-style-type: none"> 8-7 P(17) S 8-7 P(14) W 9-8 P(16) S 9-8 P(15) M 10-9 P(20) VVW 10-9 P(17) S 10-9 P(15) M 10-9 P(14) M 11-10 P(16) W 12-11 P(15) M 13-12 P(15) VW 13-12 P(13) W 14-13 P(13) W

(U) Figure 3.4
TOTAL OUTPUT RADIATION INTENSITY (WATT/CM²) (U)



UNCLASSIFIED

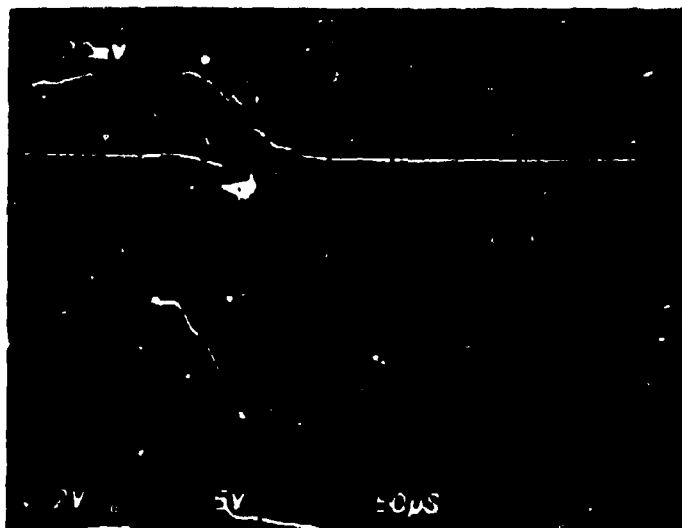


P_{tot} = 200 torr
 CO/N_2 = (1:3)
 V_{sus} = 6.3 kV
 I_{sus} = 500 A/Div

(U) Figure 3.5. Laser pulse (upper trace) and sustainer current (lower trace) for 2 kW/cc electrical pumping. (U)

UNCLASSIFIED

UNCLASSIFIED



P_{tot} = 200 torr

CO/N_2 = (1:3)

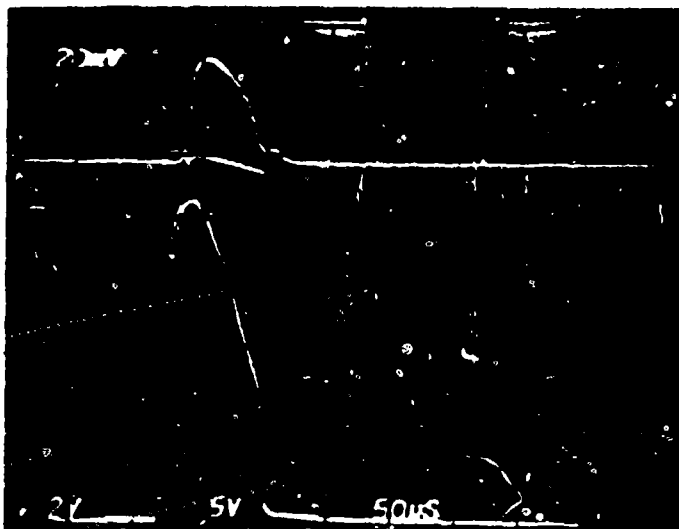
V_{sus} = 10.3 kV

I_{sus} = 500 A/Div

(U) Figure 3.6. Laser pulse (upper trace) and sustainer current (lower trace) for 6 kW/cc electrical pumping. (U)

UNCLASSIFIED

UNCLASSIFIED



P_{tot} = 200 torr

CO/Ar = (1:3)

V_{sus} = 5.4 kV

I_{sus} = 500 A/Div.

(U) Figure 3.7. Laser pulse (upper trace) and sustainer current (lower trace) for 4.4 kW/cc electrical pumping. (U)

UNCLASSIFIED

UNCLASSIFIED

CO/N₂ (1:3) with a peak electrical pumping rate of approximately 6 kW/cc. The laser pulse turn-on time ($\sim 15 \mu\text{s}$) is much shorter than that in Figure 3.5 and the energy output ($\sim 25\text{J}$) has increased by a factor of 10. The laser output from 200 torr of CO/Ar (1:3) shown in Figure 3.7 is about the same as in Figure 3.6; however, there are two significant differences between these two cases. First, the electrical excitation is only 4.5 kW/cc, illustrating that higher efficiencies are usually obtained with argon. Secondly, the long tail observed with nitrogen is not normally present with argon.

4.0 DESIGN AND CALIBRATION OF A WATER VAPOR CELL FOR LINE SELECTION

(U) The requisite of rotational spectral line selection for CO lasers and the use of a water vapor cell to accomplish this task has been discussed in previous reports.^{3-5, 7, 9, 12} Some of the design details of an existing system will be discussed in this section. This system has been used in conjunction with a low pressure-low gain CO device to study the absorptive losses introduced in the laser resonator. Some of the results of this investigation will also be presented in this Section. The absorption cell system is presently being installed in a high pressure-high gain CO device in order to investigate the line selection capability of a composite system.

4.1 The Absorption Cell. (U) The details of the absorption cell assembly are illustrated in Figure 4.1. The actual cell is constructed of stainless steel with a high temperature ceramic interior coating. It has a 2.5 cm diameter clear aperture and an optical path length of 71 cm. The Brewster windows are of calcium fluoride (Harshaw Chemical Co.) for its high transmission at 5.0 μm and its very low hygroscopicity. They are 3.0 inches in diameter and 0.375 inches thick. The windows are sealed to the cell with silicon rubber O-rings.

(U) The temperature inside the cell is sampled at four places along its length with sealed iron-constantan thermocouples (Gulton Industries Model J20M27) and monitored with a millivolt potentiometer (Leeds and Northrup Model 8686).

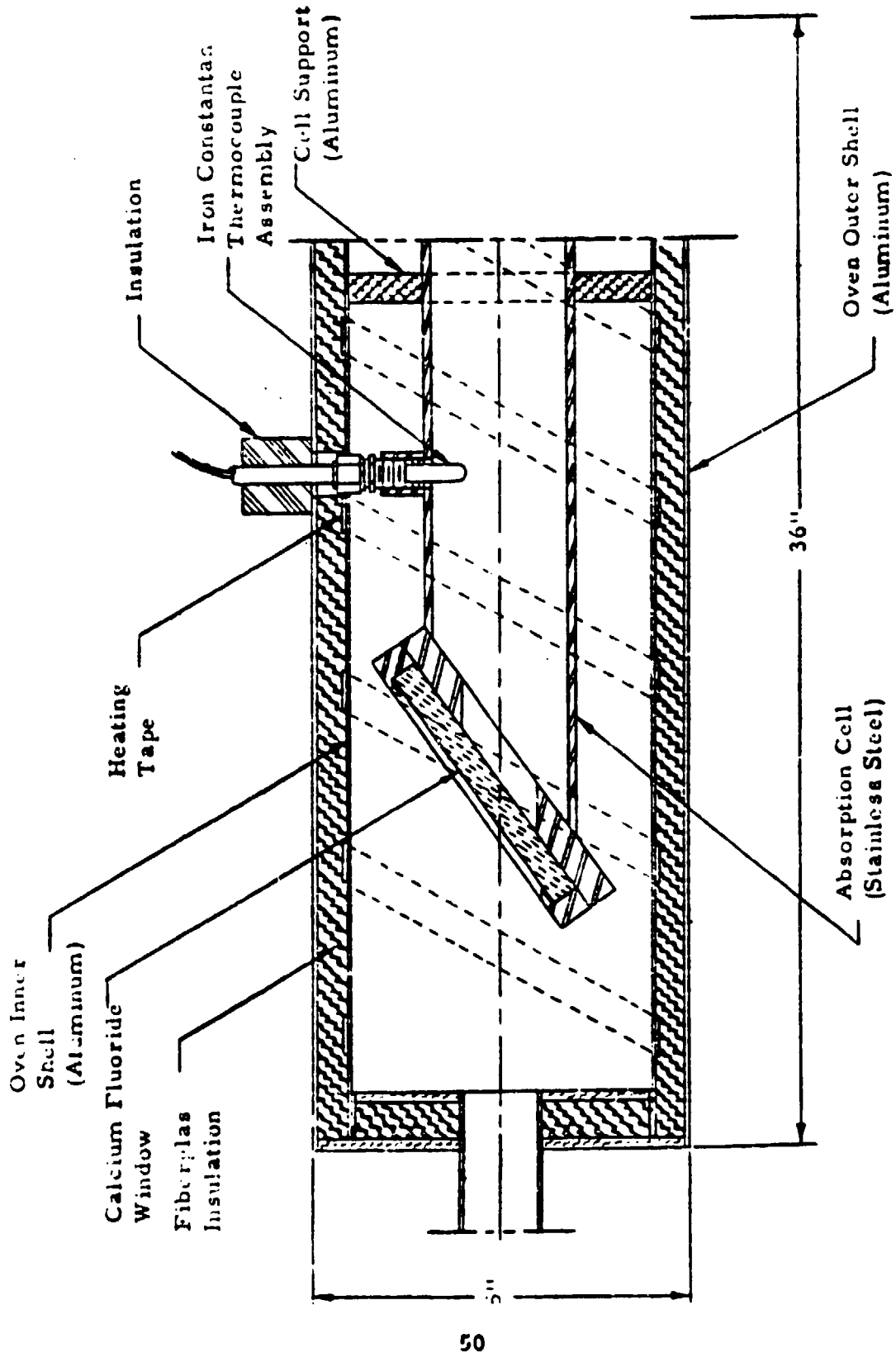
UNCLASSIFIED

(U) The oven which contains the cell consists of two aluminum shells. The inner 4.0 inch diameter shell is heated with a heater tape as shown in Figure 4.1. The input to the heater tape is controlled by a temperature controller (RFL Industries Model 70-115) using a thermister sensor placed between the tape and the inner shell. Fiberglass insulation was placed between the inner and outer shells of the oven. Each end piece of the oven consists of two circular phenolic discs separated by fiberglass insulation and connected by a 1.0 inch i. d. aluminum tube which extend 6.0 inches beyond the oven end. The temperature inside the cell can be varied from 25°C to 200°C and a uniform temperature from one end to the other can be maintained to $\pm 2^\circ\text{C}$. The cell is supported in the oven at two places by aluminum spider mounts. The thermocouple extensions from the oven are wrapped with a foam rubber insulation.

(U) The plumbing system for the absorption cell is illustrated in Figure 4.2. All of the tubing used in the system is of stainless steel. All valves are stainless steel bellows type (Nupro Co.). A liquid nitrogen cold trap was installed between the vacuum pump (Duoseal Model 1400) and the cell to prevent damage to the pump when evacuating water vapor from the cell.

(U) The pressure in the cell is monitored with a high temperature differential pressure transducer (Viatran Model No. 304) in conjunction with a signal conditioner (Action Instruments Model 4051) and a digital voltmeter (Trymetrics Corp. Series 4000). For cell pressure up to 50 psia, a vacuum pump (Duoseal Model 1400) is connected to the reference side of the transducer. The transducer monitoring system was calibrated against two accurate pressure gauges (Wallace and Tiernan 0 - 800 torr and Wallace and Tiernan 0 - 100 psi). The calibration curves were determined at all of the various operating temperatures.

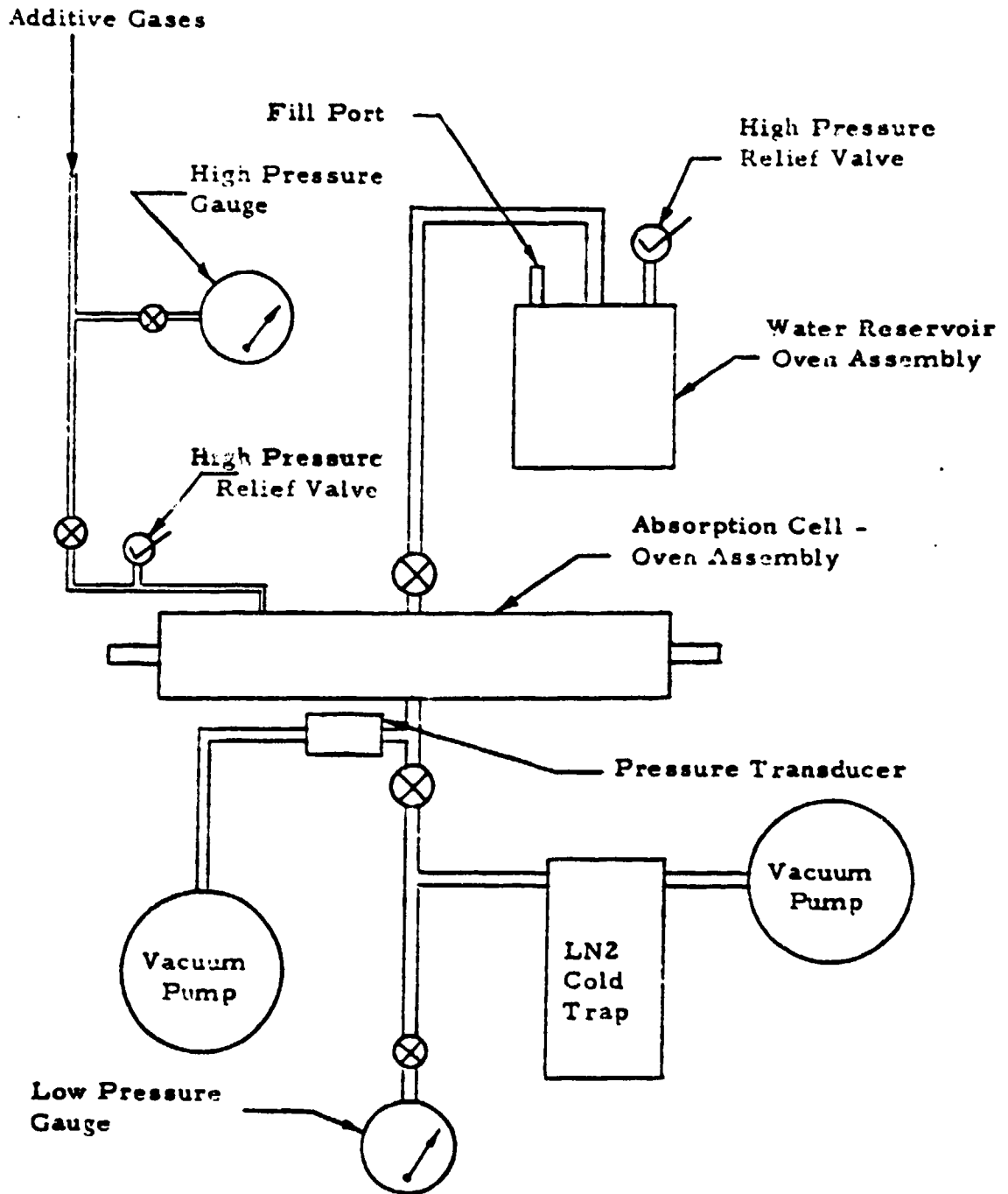
UNCLASSIFIED



(U) Figure 4.1. Absorption cell - oven partial assembly. (U)

UNCLASSIFIED

UNCLASSIFIED



(U) Figure 4.2. Absorption cell system for CO laser spectral line selection investigation. (U)

UNCLASSIFIED

UNCLASSIFIED

(U) The water reservoir is 4 inches in diameter and 8 inches long. It is constructed of stainless steel with a high temperature ceramic interior coating. The reservoir is heated with a band heater which is controlled by a temperature controller (RFL Industries Model 70-115) using a thermistor sensor placed between the band and the reservoir. The reservoir is enclosed in an aluminum shell 7 inches in diameter and 11 inches long. Fiberglass insulation is placed between the reservoir and the shell.

A line to an external gas manifold to provide the capability of adding gases other than water vapor is included. High pressure relief valves have been installed on the reservoir and on the external gas line to prevent over pressures in the system.

(U) The cell pressure can be varied from 0.01 torr to 5 atmospheres. The system can provide water vapor up to 2 atmospheres and additional absorbing or broadening gases can be introduced to a total pressure of 5 atmospheres.

(U) The external gas line, the water reservoir line, and the pressure transducer line are heated with heater tapes and insulated with an epoxy-foam. The tapes are controlled with temperature controllers (RFL Industries Model 70-115) using thermistor sensors. Since water vapor in the system will condense at points with a lower temperature than that of the water vapor, the external lines are kept at a higher temperature than that of the cell or the reservoir.

UNCLASSIFIED

4.2 Calibration and Absorption Measurements. (TT) It has been previously demonstrated^{3,9} that a water vapor cell internal to a low pressure-longitudinal discharge CO laser would tend to limit laser action in a particular vibrational band to those rotational lines having high transmission through the atmosphere. It is desirable to optimize this approach for low pressure lasers and to utilize it in high pressure-high gain CO lasers. This requires the determination of the actual intracavity loss introduced by the water vapor content, temperature, and additive broadening gases. An investigation was undertaken to experimentally measure the monochromatic absorptive losses introduced by an intracavity water vapor cell as a function of various parameters, and to correlate the results with calculated values in order to determine the applicability of existing theoretical models. During the course of the investigation, the changing of the various parameters necessarily involved the calibration of the absorption cell system.

(U) The experimental layout for measuring the absorption coefficients and for calibration of the cell was described briefly in an earlier report.⁵ Details of this configuration are presented in a separate report⁸ which also contains all of the investigatory results to date. This data compliments that of the preliminary report.^{7,12} A summary of this investigation is discussed in this section.

(U) The CO spectral frequencies studied were limited to rotational lines in the vibrational bands 7-6 to 10-9. Low pressure-longitudinal discharge lasers exhibit extremely low gain for laser frequencies corresponding to v-bands lower than 6-5. With the additional loss introduced by the diffraction grating for the configuration used in this study, laser action was not obtained on the lower v-bands. The theoretical studies of

UNCLASSIFIED

McClatchey¹⁰ and NLS⁵ indicate that only lines in the spectral region encompassed by vibrational bands 1-0 to 6-5 are of value for atmospheric propagation. However, the information gained by studying the higher vibrational band lines will help define the optimum configuration for line selection in the lower bands.

(U) Absorptance losses were measured for 20 CO laser lines for various sets of conditions. These losses were compared to calculated results obtained using a computer code developed at NLS and utilizing existing theoretical models. All of the data points to date have been for a vapor cell temperature of 150°C. The largest absorptive loss which could be measured was 37%. This limited the water vapor content of the cell for this investigation. The effects of water vapor contents of 100, 200, 250 and 325 torr were measured. CO₂ and N₂ gases were added in pressures up to 4 atm in order to examine the broadening effects of these gases. In addition, absorptance effects of CO₂ were measured. The theoretical values for CO₂ could not be calculated because the pertinent parameters for CO₂ absorption are not available in the published literature. These parameters have been computed, tabulated, and recorded on magnetic tape at the Optical Physics Laboratory at AFCRL; however, this information will not be made available to requesters until January 1973.²⁰

(U) A typical set of data is shown in Table 4.1. The water vapor content is 200 torr and the amount of N₂ as a broadening gas is 2 atm. $\delta(\text{H}_2\text{O})$ is an absorber length representation for the water vapor and is just the vapor density multiplied by the path length. The KL values are those given by the Beer's law expression for the absorptance; i. e., $A = 1 - \exp(-KL)$. The $>$ symbol signifies the loss introduced was greater than that which

UNCLASSIFIED

(U) Table 4.1. Water vapor absorptive losses for CO laser radiation due to an intracavity vapor cell. (U)

$P(\text{H}_2\text{O}) = 200 \text{ torr}$
 $P(\text{N}_2) = 1520 \text{ torr}$
 $P(\text{CO}_2) = 0 \text{ torr}$
 $T = 153^\circ\text{C}$
 $\delta(\text{H}_2\text{O}) = 3.234 \times 10^{20} \text{ molecules/cm}^2$

CO LASER SPECTRA		ABSORPTANCE		KL	
Identification	Frequency (cm^{-1})	Measured	Calculated	Measured	Calculated
10-9 Band					
P(14)	1854.921	0.111	0.067	0.118	0.069
P(10)	1870.607	>0.365	0.934	>0.454	2.725
P(9)	1874.445	0.106	0.075	0.112	0.078
P(9)	1878.249	0.117	0.084	0.124	0.088
P(7)	1882.020	0.072	0.046	0.075	0.047
9-8 Band					
P(14)	1880.336	0.103	0.093	0.109	0.097
P(13)	1884.342	>0.365	0.421	>0.454	0.546
P(12)	1888.315	>0.365	0.359	>0.454	0.445
P(11)	1892.255	0.307	0.192	0.367	0.214
P(10)	1896.162	>0.365	0.239	>0.454	0.273
P(9)	1900.035	0.059	0.042	0.061	0.043
P(8)	1903.875	0.160	0.125	0.174	0.133
8-7 Band					
P(14)	1905.829	0.108	0.068	0.114	0.070
P(12)	1913.878	0.168	0.101	0.184	0.107
P(10)	1921.794	>0.365	0.621	>0.454	0.970
P(9)	1925.703	0.142	0.088	0.153	0.092
7-6 Band					
P(14)	1931.396	0.064	0.037	0.066	0.038
P(13)	1935.473	0.083	0.203	0.087	0.226
P(12)	1939.516	0.129	0.089	0.138	0.093
P(10)	1947.503	0.089	0.074	0.093	0.077

UNCLASSIFIED

could be measured. As seen from the data in the table, the measured losses are always greater than those predicted by the theory. The exception to this statement is the 7-6P(13) line. The explanation for this anomaly was presented in the preliminary report;^{7,12} it involves a mis-labeled water vapor absorption line location.

(U) A comparison of the measured and calculated values for various sets of parameters indicates that for low water vapor content (< 100 torr) the theoretical model provides a reasonable description of the absorption mechanisms with or without N_2 or CO_2 . As the water vapor content is increased, the theoretical model becomes less and less adequate in describing the absorption loss. The conclusion reached is that the currently existing theories provide a reasonable description of the broadening effects of CO_2 and N_2 but do not reasonably describe the self-broadening effect of water vapor.

(U) It was determined that the monochromatic water vapor absorptive losses (KL) can be increased by the addition of a broadening gas, thus increasing the differential loss (ΔKL) between two CO rotational lines in a v-band. However, the addition of water vapor has a more significant effect by increasing the absorber length (δ) and by the self-broadening effect. This second effect is much more than would be predicted by existing theory.

UNCLASSIFIED

5.0 AREA CATHODE E-GUN DEVELOPMENT

(U) The CO laser devices currently under development require large area E-guns capable of high current density with good beam uniformity. Several approaches for satisfying these requirements have been investigated and tested using small scale prototypes and a full scale gun has been designed and is under construction.

(U) The large area electron gun, which will have beam dimensions of 10 cm x 100 cm, is designed to provide a minimum current density of 100 mA/cm² at 300 kV. To simplify electron optics and to assure current density uniformity, a large area cathode of the barium oxide impregnated porous tungsten type has been adapted to the NLS design. The cathode, of identical size as the E-beam dimensions, results in a planar electrode geometry and prototype tests have shown a tetrode electrode configuration to be best suited for beam control.

The two grids, a control grid and a screen grid, enable the current density to be controlled independently of the E-beam acceleration potential. The planar electrode geometry and space charge limited operation assure current density uniformity over the beam area.

Prototype testing with a 9 cm diameter disk cathode has demonstrated the applicability of the impregnated cathode to large area E-beam guns. The tests have also provided design data from which the scaled up 10 cm x 100 cm E-gun is being designed and fabricated.

5.1 Impregnated Cathode Characteristics. (U) The attractive feature of the impregnated cathode is the low work function, 1.67 eV, of its barium oxide coated surface. Emission densities of 1 A/cm² are possible at temperatures of 950°C.

UNCLASSIFIED

(U) The porous tungsten matrix (approximately 20% porosity) serves as a BaO reservoir which continually replenishes any BaO evaporation from the cathode surface. For this reason, the impregnated cathode can be reactivated after exposure to the atmosphere. At the expected operating temperatures of 900 to 950°C the amount of BaO evaporation is immeasurably small and cathode life is on the order of 10^5 to 10^6 hours.

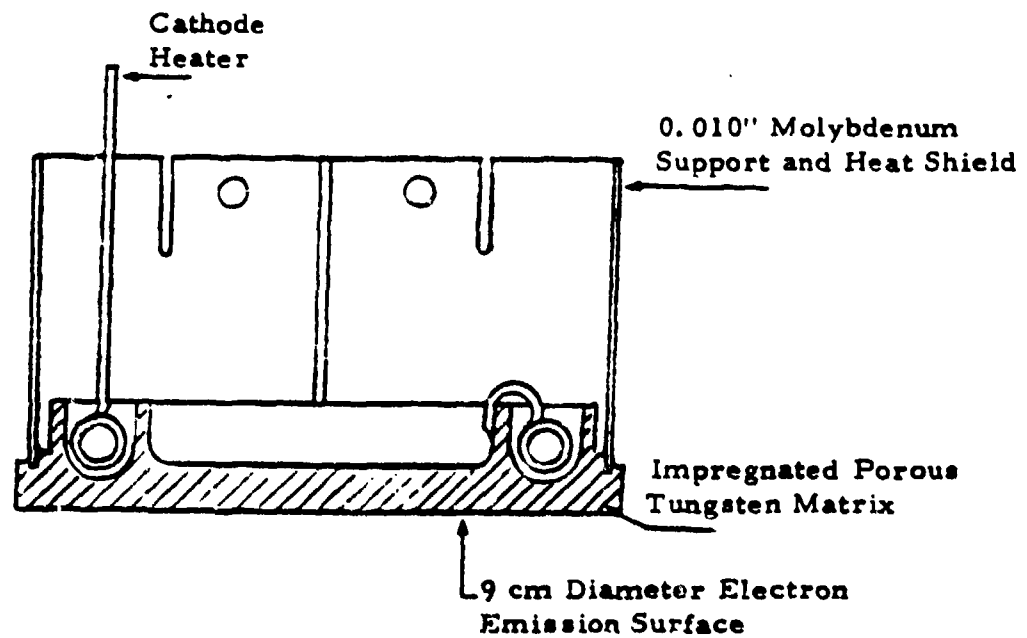
5.2 Prototype Tests. (U) To evaluate the area cathode concept, extensive tests were performed with a 9 cm diameter disk cathode. The emitting surface of the cathode was flat while the reverse side contained a molybdenum heater potted in alumina and mounting skirt of 0.10 inch thick molybdenum. The cathode cross section is illustrated in Figure 5.1.

Cathode Activation and Exposure to air while Hot. (U) To achieve rated performance from an impregnated cathode which has been exposed to air, it is necessary to activate the cathode. Activation involves recoating of the emitting surface with BaO and this is accomplished by heating the cathode to 1200°C for approximately 30 minutes or to a lesser temperature for longer periods.

(U) Experience gained from the prototype cathode showed the impregnated cathode to be reliable for reactivation. A variety of electrode configurations were investigated which required that the vacuum system be opened frequently. After exposure to air, emission was achieved by activation at temperatures above those required for the desired emission level. At lower current densities, 1 to 10 mA/cm², activation to only 1050°C was adequate. Also, prolonged operation at 950°C had a similar effect as a shorter higher temperature activation.

UNCLASSIFIED

UNCLASSIFIED



(U) Figure 5.1. 9 cm Disk Cathode. (U)

UNCLASSIFIED

UNCLASSIFIED

(U) The vacuum load on the pumping system was substantial for a cathode which had been exposed to air. While heating up for activation, the heating rate had to be regulated to keep the pressure below 5×10^{-6} torr. After activation, however, the hot cathode had virtually no effect on the system base pressure, which was 5×10^{-7} torr.

(U) To establish the ability of the cathode to be reactivated after a window rupture, while the cathode was hot, a simulation was performed. With the cathode at 950°C , the vacuum system gate valve was closed and the up-to-air valve was opened, venting laboratory air into the system. Approximately 3 seconds after opening the valve, an appropriate time for interlock response on a large system, the cathode heater power was cut off. The cathode had the appearance of being oxidized after this treatment. On the recommendation of the cathode manufacturer, the emission surface was sanded with #200 alumina grit sandpaper. This was done until the cathode had the same matte metallic luster as before the hot exposure.

(U) Activation following the usual procedure yielded the same level of performance as experienced before the hot up-to-air exposure. This test demonstrated the ability of the cathode to survive a window rupture while hot.

Diode Tests. (U) In its simplest form, because the cathode can be fabricated to the E-beam dimensions, the E-gun could have been a diode, with the anode being the gun window. Diode tests were performed with the prototype cathode to measure beam uniformity, the most important performance parameter for a diode gun. Temperature limited operation is the most practical method for controlling current density if it is to be independent of acceleration potential, for a fixed cathode-anode spacing.

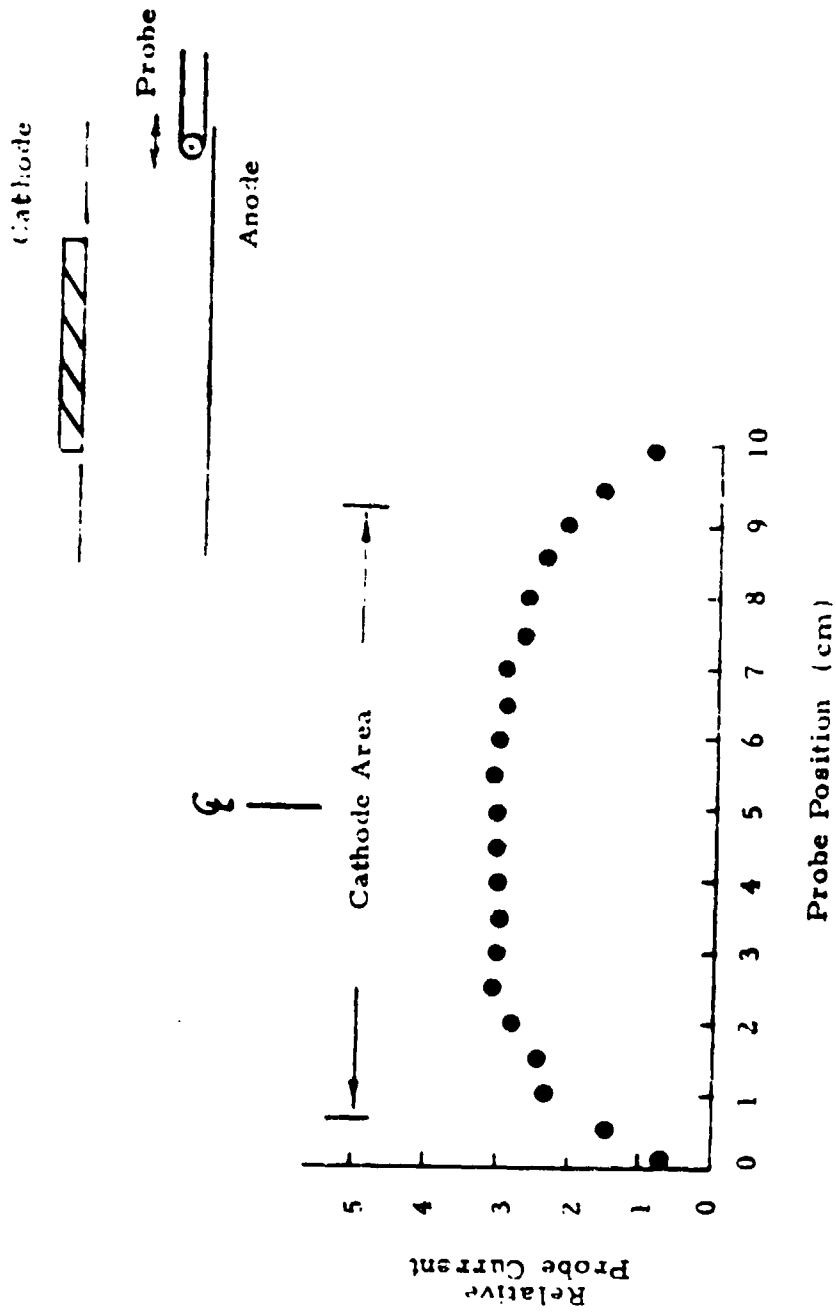
UNCLASSIFIED

(U) Using a movable Faraday current probe, current uniformity was measured, with the cathode operated both space charge limited and temperature limited. Typical space charge limited results are presented in Figure 5.2, where the probe current, in relative units, is plotted against probe position. The cathode centerline corresponds to the 5 cm position and the cathode diameter spans the measurement as indicated. In the central 4 cm the space charge limited current can be seen to be quite uniform while the fringing fields on the periphery cause a trailing off of the current distribution. Probe measurements at higher cathode-anode biases, when the diode was operating temperature limited, revealed considerable current nonuniformities which could be correlated to a temperature nonuniformity.

(U) Because of the exponential dependence of the Richardson equation, cathode temperature uniformity would have to be held to tolerances of $\pm 5^{\circ}\text{C}$ for temperature limited operation. This is impractical and diode operation was rejected as a versatile E-gun design.

Gridded E-Gun: Tetrode Configuration. (U) To assure a high degree of current uniformity and to allow precise control of the E-gun current, it was necessary to decouple the functions of current extraction and electron acceleration. The prototype cathode was tested in a tetrode configuration, as illustrated in Figure 5.3.

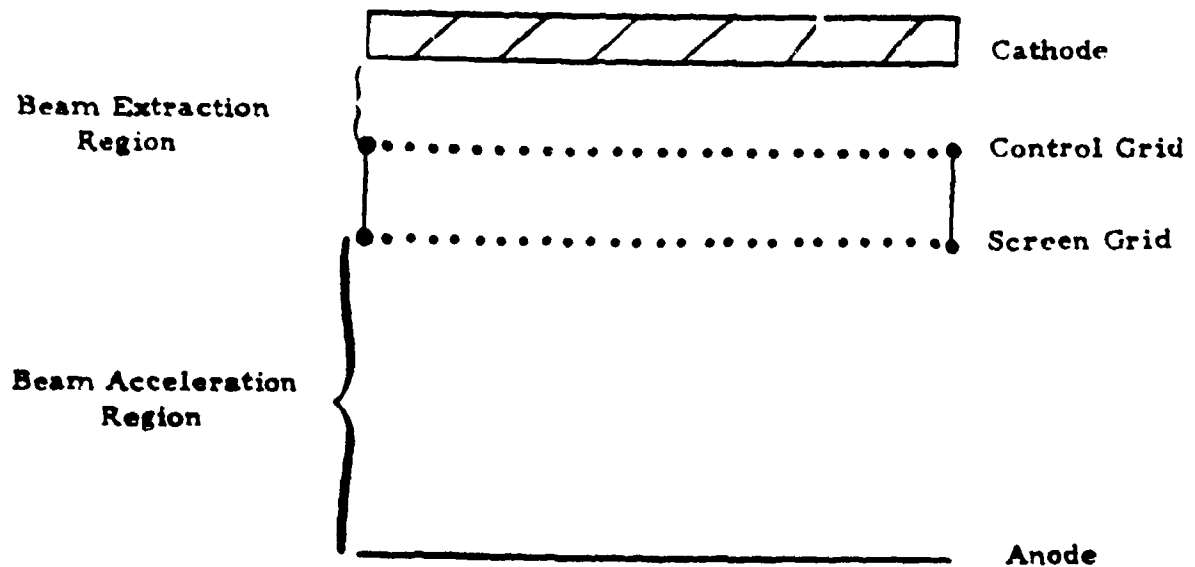
(U) Typical acceleration fields will be as high as 20 kV/cm while the extraction fields are 1 kV/cm or less. The beam formation region, which is actually the cathode-control grid region, is shielded from the acceleration fields by a screen grid. The screen grid is at the same potential as the control grid and, although there is some field penetration into the control screen grid gap, there is none into the control grid-cathode gap. Thus, the



(U) Figure 5.2. Area cathode current profile for diode geometry. (U)

B

UNCLASSIFIED



(U) Figure 5.3. Tetrode E-gun electrode configuration. (U)

UNCLASSIFIED

gun current density is controlled by the cathode-control grid bias and the electron energy can be selected independent of that control voltage.

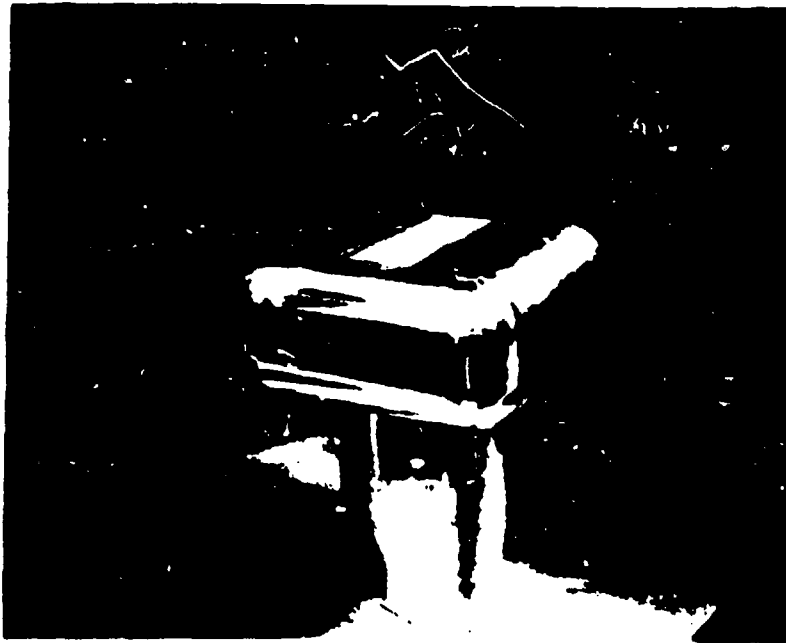
(U) This configuration tested quite satisfactorily with the 9 cm diameter disk cathode. Part of the cathode was masked off to form a 4.5 cm x 8 cm rectangular cathode. Control and screen grids were fabricated from stainless steel wire mesh and positioned 1 cm away from the cathode. The control to screen grid spacing was 1 cm and the combined grids had a transmission of 60%. These electrodes were mounted inside a high voltage terminal to entirely shield the cathode, and an anode was positioned 1.5 cm from the screen grid. This entire assembly was mounted inside a glass tee, diffusion pumped vacuum system. Typical operating pressures were approximately 5×10^{-7} torr.

(U) The cathode, control and screen grid spacings will be the same in the 10 cm x 100 cm gun. The acceleration region was purposely made small so that typical acceleration fields could be duplicated with voltages of 25 kV or less.

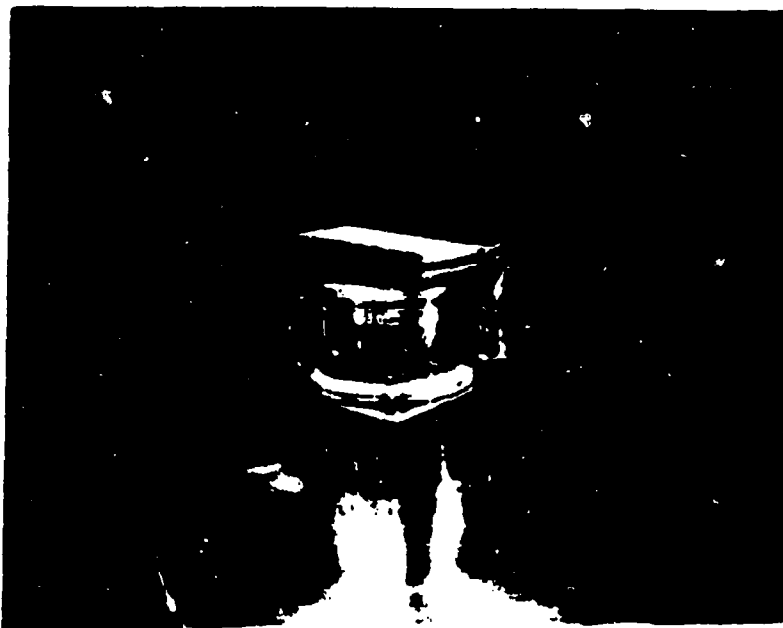
(U) Figure 5.4 shows two photographs of the prototype gun. The top photograph shows the high voltage shroud mounted on the vacuum flange. The beam area is the mesh covered area. The bottom photograph shows the gun partially disassembled. The impregnated cathode, supported by a 0.010 inch molybdenum skirt, can be seen along with the control and screen grid structure.

(U) To check the independence of the gun current upon the accelerating bias, the gun current was measured for biases from 5 to 25 kV. These voltages correspond to fields from 3.3 to 15.7 kV/cm. These results are plotted in Figure 5.5 where it can be seen that the anode current varied

UNCLASSIFIED



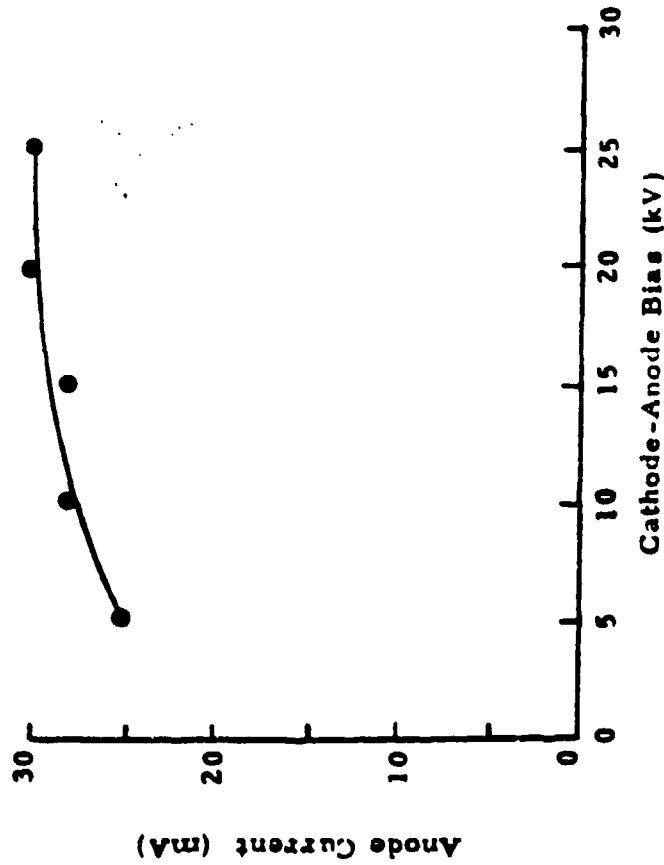
Prototype E-gun illustrating the beam area and high voltage terminal. (U)



Partially disassembled prototype E-gun illustrating the area cathode and control grids. (U)

(U) Figure 5.4

UNCLASSIFIED



(U) Figure 5.5. Anode current dependence upon cathode-anode bias. (U)

UNCLASSIFIED

less than 10% for the 5-fold variation in electron energy. This data, along with similar data at other current densities, demonstrates that current control is independent of the accelerating voltage.

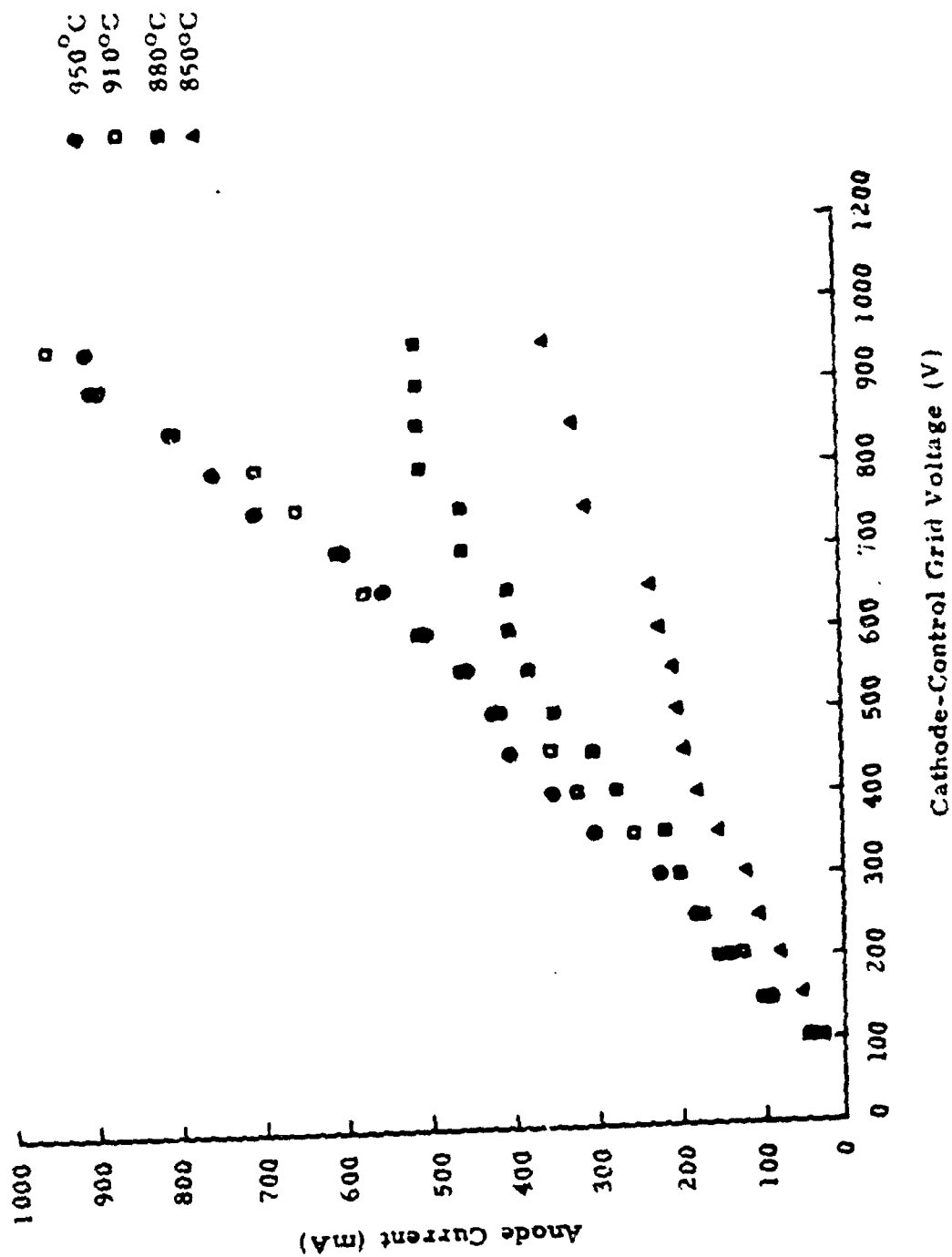
(U) The E-gun current density control was studied by measuring the anode current as a function of the cathode-control grid bias. This data is plotted in Figure 5.6 as a function of cathode temperature. The 950°C and 910°C data follow a Child's Law dependence, increasing to 1 amp of pulsed current. This corresponds to an anode current density of 28 mA/cm², or essentially 50 mA/cm² of extracted cathode current when account of grid current is taken.

(U) The limitation on anode current was imposed by the grid circuit pulse generator which only went to 950 volts. Since the curves are increasing, and the impregnated cathode should emit substantially more current at these temperatures, it can be assumed that anode current densities of 100 mA/cm² are readily available.

(U) It should be noted that since the 950°C and 910°C data are identical, the gun is indeed operating in the space charge limited mode. At lower cathode temperatures, the 880°C and 850°C data, the low current region is also space charge limited. However, the 880°C data falls off and becomes temperature limited at approximately 500 mA and the 850°C data becomes temperature limited at 300 mA. For current densities of 10 mA/cm² or less, these are suitable operating temperatures. Results from these prototype tests have provided the basis for scaling up the E-gun dimensions to the desired 10 cm x 100 cm beam size.

5.3 Large Area Cathode E-gun. (U) The overall configuration of the large area cathode design which is being fabricated at the present time is illustrated in Figure 5.7. The essential elements are the high voltage

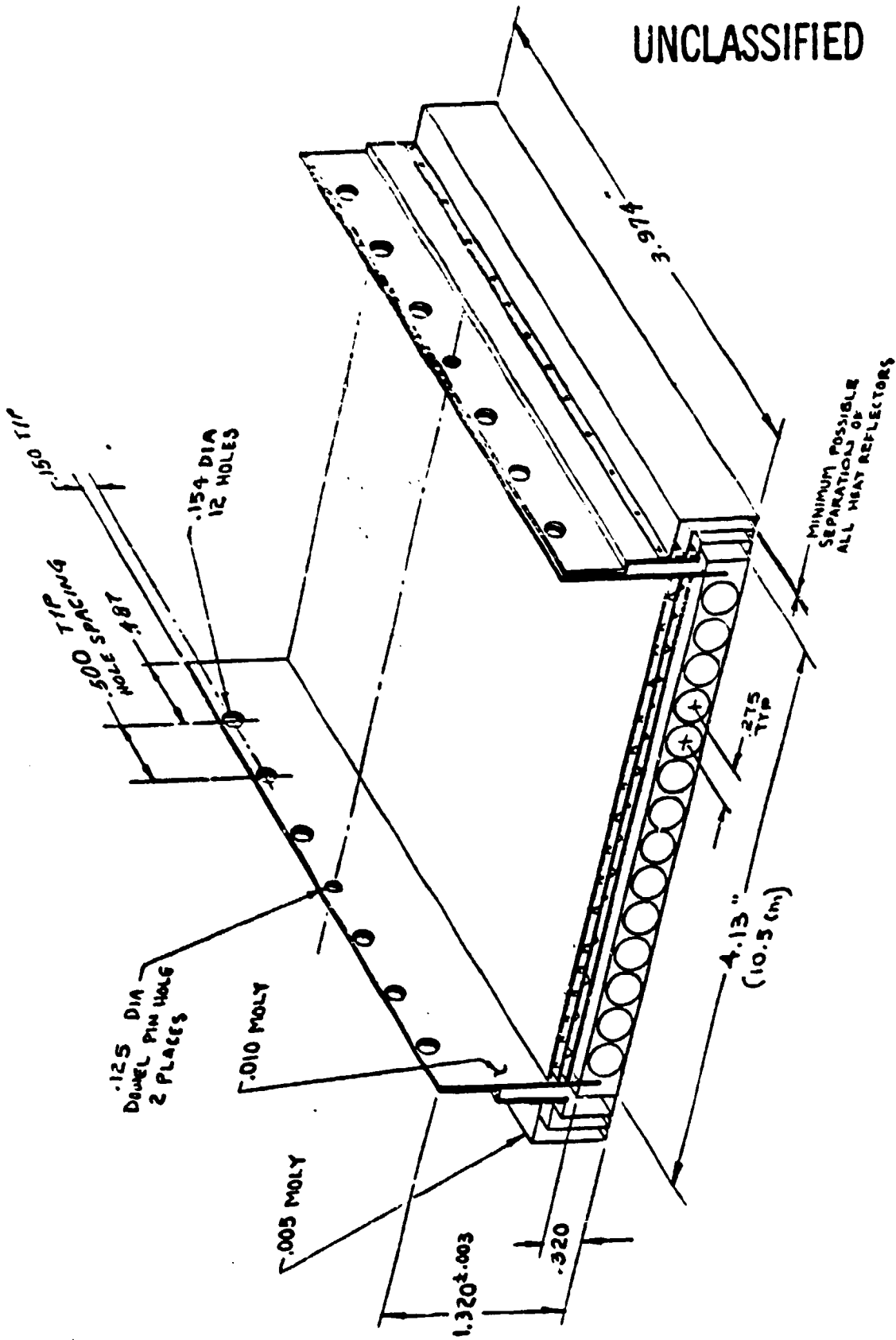
UNCLASSIFIED



(U) Figure 5.6. Anode current dependence upon cathode control grid pulse voltage. (U)

UNCLASSIFIED

UNCLASSIFIED



(U) Figure 5.7. Design details of cathode segment. (U)

UNCLASSIFIED

UNCLASSIFIED

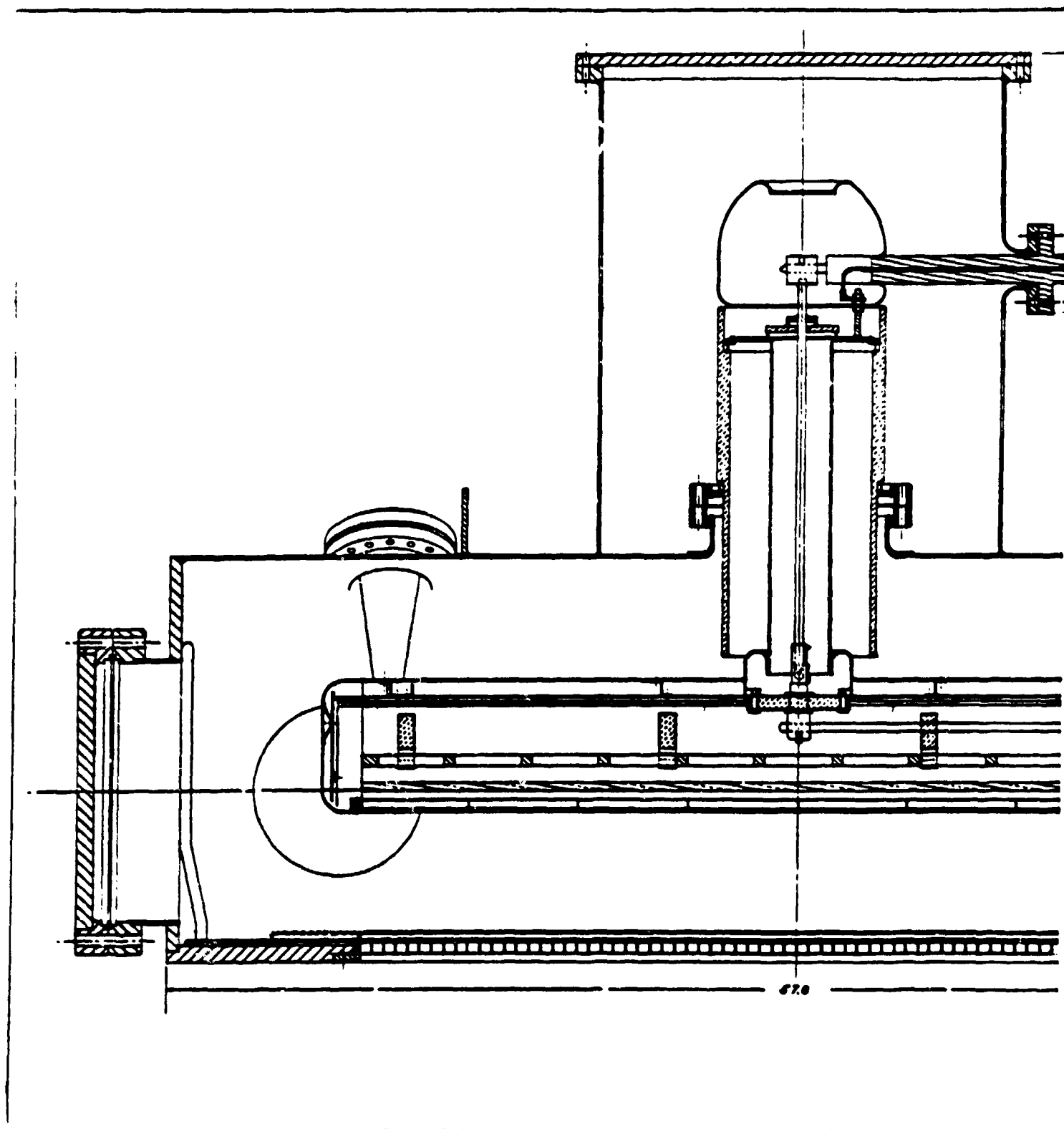
terminal which houses the cathode, the control grid and screen grid, the window, the vacuum envelope, and the high voltage feedthrough.

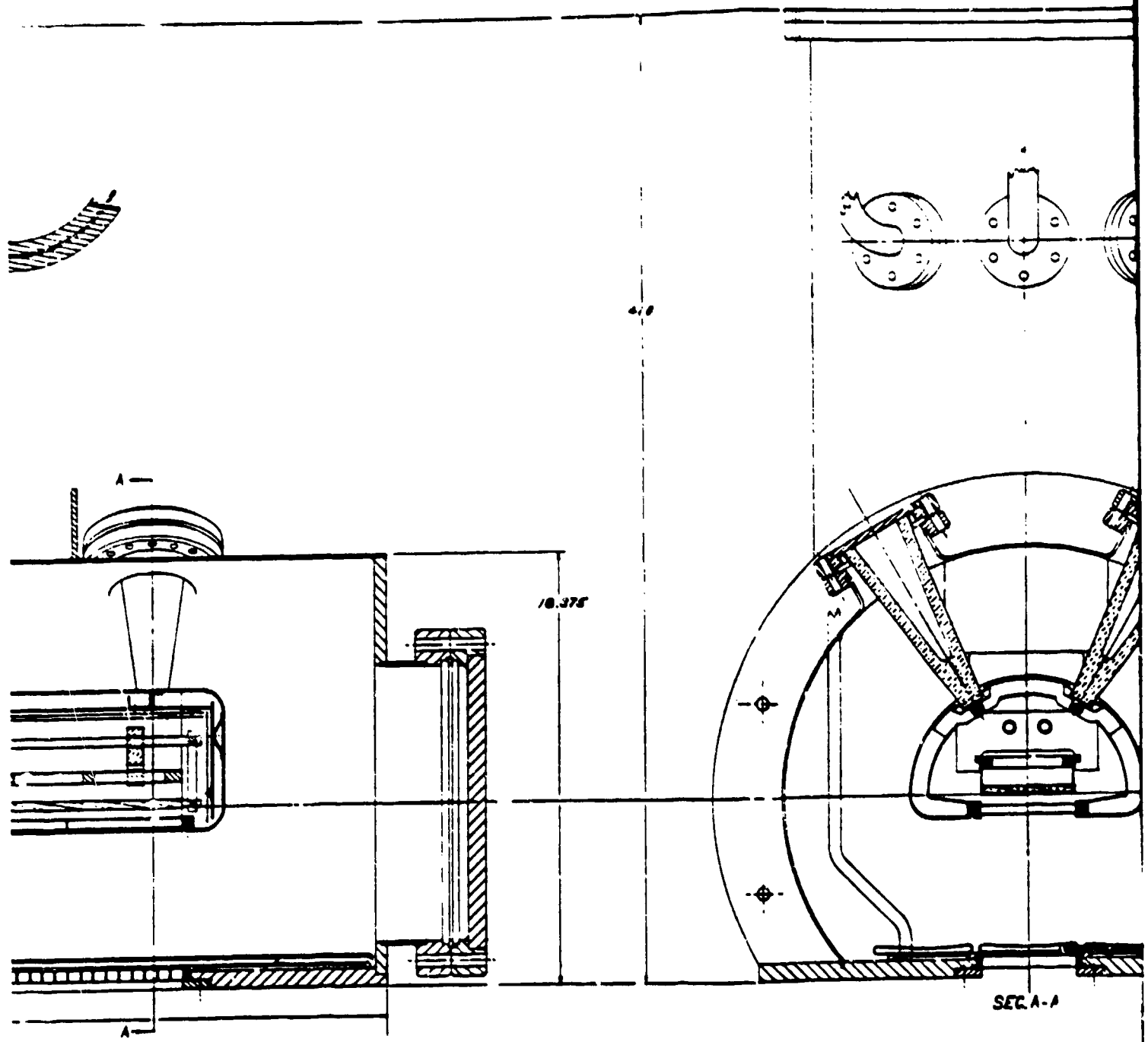
High Voltage Terminal. (U) The E-gun electrodes, consisting of the cathode, the control grid, and the screen grid, will be supported inside a high voltage terminal, which will be electrically insulated from ground. The terminal will be concentric with the vacuum chamber and its cross section, illustrated in Figure 5.7, is shaped to prevent excessive fields (and thus breakdown) and also to shield the cathode-control grid region. All of the beam formation will be done within the terminal and the acceleration will be done between it and the gun window.

(U) Details of the cathode construction are illustrated in Figures 5.7 and 5.8. The 10 cm x 100 cm cathode will be fabricated from 10 cathodes of dimensions 10.5 cm x 10.2 cm. This will give 0.25 cm overhang on the width and 1 cm overhang on the length to take account of end losses. The cathodes will be supported by 10 mil molybdenum skirts, which will be brazed to the cathode and screw-connected to a support stringer. Tungsten heaters, the length of the entire assembly, will be inserted into the holes provided. The top and sides of the cathode assembly will be heat-shielded to prevent excessive thermal radiation.

(U) The cathodes will be fabricated by Spectra-Mat, Inc. of Watsonville, California. They have extensive experience in impregnated cathode fabrication and have already made cathodes of the size and configuration.

(U) The cathode assembly is inserted into the high voltage terminal via the alumina insulators which position the cathode and electrically insulate it from the terminal. Power for the cathode heater





10

is brought out to the end of the terminal where it is connected once the cathode is in position. This enables complete removal of the cathode from one end of the vacuum chamber without necessitating the dismounting of an attached laser.

(U) The control-screen grid assembly will be fabricated from molybdenum wire, 20 mil diameter, continuously wound in a shadow grid configuration on molybdenum rods. The grid wire pitch will be 0.2 cm resulting in a 80% transparent configuration. The grid structure will also be inserted into the terminal as illustrated in Figure 5.8.

(U) The high voltage terminal will be fabricated using a double walled configuration of 20 mil inside and 50 mil outside stainless steel. Periodic ribs will provide a light but rigid structure. Support will be provided by alumina insulators, as illustrated in Figure 5.8, so that the gun can be operated in either a horizontal or vertical orientation. The high voltage bushing will not carry any of the gun weight.

(U) Connection to the heater power and the grid control circuits will be through high current (250 amp rated) pin socket fittings. To assemble the gun, the high voltage terminal will be inserted into the vacuum chamber, inserted onto the bushing electrodes and then pinned in place on the high voltage support ceramics.

E-Gun Vacuum Chamber. (U) The high vacuum chamber will be fabricated from stainless steel, all feedthroughs will be of the brazed ceramite-co-metal type, and all flanges will be metal gasketed. The single exception will be the E-beam window, which will be Viton "O"-ring sealed. This method of fabrication is consistent with good vacuum practice and should assure gun operation in the 10^{-7} torr region.

UNCLASSIFIED

(U) Experience with the prototype test gun shows that the impregnated cathode is inherently a clean material. Operating in a teflon gasketed glass tee evacuated by oil diffusion pumps, the cathode hot pressure was 3×10^{-7} torr, which was the system base pressure. With an all metal system and appropriate pumping, base pressure operation should be in the 10^{-8} torr range with cathode hot operation well below 10^{-6} torr.

(U) The vacuum chamber will be fabricated from 1/8 inch thick 304 stainless steel which has been cylindrically rolled and heliarced to the window flange, as shown in Figure 5.8. Periodic ribs heliarced on the outside will provide stiffening. The cylinder diameter is 21 inches and the length is approximately 60 inches. This method of fabrication should yield a light (approximately 400 pounds) but strong vacuum chamber. Access for gun installation and servicing will be through the two 14 inch end ports. For convenience, pumping will be through a side entrant port giving free access to the gun without the need of vacuum pump removal.

(U) A thermal analysis of the cathode and gun configuration predicts an entire heat load of approximately 4 kW from the area cathode. This corresponds to a cathode specific heat load of 4 W/cm^2 . These calculations are consistent with the prototype tests where the specific heat load was 6.5 W/cm^2 . These tests were performed with heat shielding suitable for the prototype gun, but inadequate for a full scale gun.

(U) Heat loads in the window region will be on the order of 0.4 W/cm^2 . To protect the window and to keep the Viton seal cool, water cooling channels run the length of the window flange. Additional protection is provided by a shutter, which will cover the window when the gun is biased off. When the gun is pulsed, the shutter will be moved to a position over the coolant channel, the gun will be pulsed on, and the shutter will be returned to the

closed position. To assure vacuum integrity, the shutter activating mechanism will be driven by a linear-motion bellows-sealed feedthrough, mounted on a copper gasket sealed flange. A dummy shutter on the opposite side of the chamber will assure field symmetry.

(U) The thermal analysis also indicates that the outer shell of the high voltage terminal will reach an equilibrium temperature of approximately 250°C during extended gun operation. The pinned support method of mounting will allow axial expansion of the high voltage terminal to assure dimensional stability.

Window and Support Structure. (U) The two conflicting requirements of low electron energy loss in the window and a 2.5 atmosphere pressure differential across the window necessitate compromise in its design. No 10 cm x 100 cm window can be self-supporting, so it is necessary to provide periodic support. Suitable window material could be either aluminum or titanium, although the latter is preferable. The rate of electron energy loss is approximately double in titanium what it is in aluminum. However, titanium is more than twice as strong as aluminum so it is the preferred window material for this application.

(U) The window material and support scheme to be used in the proposed gun have already been tested and used in practice in a 5 cm x 100 cm configuration. The window has been demonstrated to be sturdy and reliable under operating extremes of pressure transients (to 3 atmospheres) and when exposed to cryogenic gases (100°K). Static tests have been conducted up to overpressures greater than 4 atmospheres without window rupture.

UNCLASSIFIED

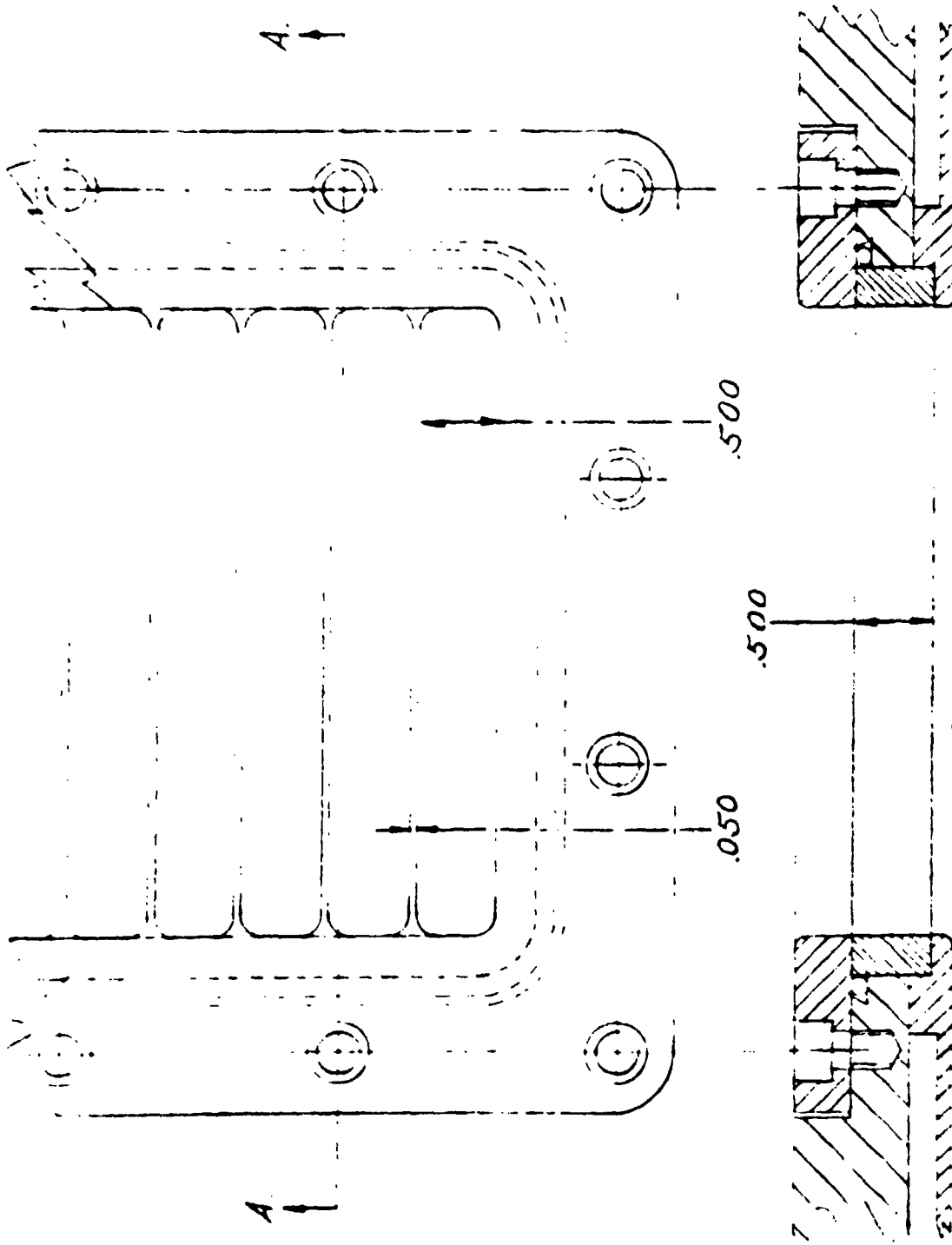
(C) The window material will be 0.001 inch thick titanium foil supported by a periodic structure as illustrated in Figure 5.9. Experience in our laboratory has shown this to be a rugged window of acceptable energy loss. Calculations of the average energy loss give 10 keV at 200 keV and 40 keV at 120 keV.

(D) The support structure will be machined out of a solid piece of stainless steel to assure dimensional integrity. The support webs will be 32 mils thick by 1/2 inch high and they will be on 0.55 inch centers. This corresponds to a 90% transmission support. Figure 5.9 illustrates details of the support design.

(E) The support webs completely stop all electrons which strike them, but this does not have the effect of making the current density nonuniform. Window scatter washes out the support web absorption. The electron scatter distribution function can be approximated by a Gaussian with a mean angle of scatter of 25° . A NLSD computer program developed to evaluate the electron current density shows that at distances of 2 cm or more from the window the current density variation is insignificant. The data, plotted in Figure 5.10 shows the current density at various distances away from the window. These calculations did not take account of gas scattering, which will contribute as much to beam smoothing as window scatter. Thus, even at 1 cm from the window, the beam will be uniform to within 5% (i. e., the 2 cm results in Figure 5.10 are valid at 1 cm when gas scattering is included).

(F) The window support assembly will be held in position independent of the window itself. This makes window replacement more convenient and it assures precise positioning of the supports. Window replacement will be done simply by laying a new foil over the window flange and inserting it into the gun window flange. The "O"-ring will be held in place, for horizontal operation, by a tapered groove. The window will be secured to the window flange by two pins to hold it in place while mounting.

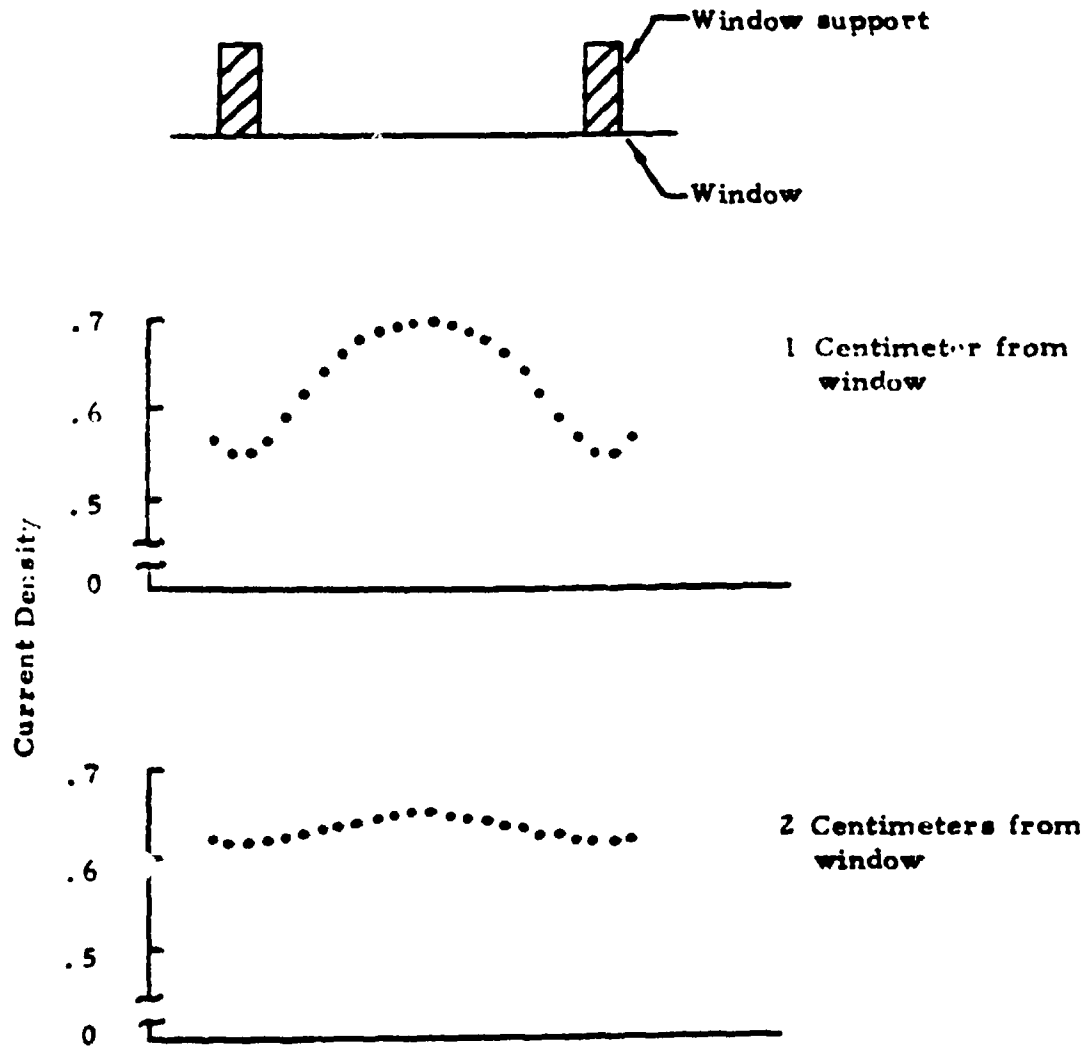
UNCLASSIFIED



(U) Figure 5.9. Window Mount and Support Detail. (U)

UNCLASSIFIED

UNCLASSIFIED



(U) Figure 5.10. Effect of window scatter upon E-beam uniformity. (U)

UNCLASSIFIED

High Voltage Termination. (U) The E-gun and the power supply will be interconnected by three cables which will supply the negative high voltage bias, the cathode heater power, and the control grid modulation voltage. The cables will be of the coaxial shielded type terminating in oil at the power supply and in SF₆ at the gun.

(U) The gun electrical services will be brought into the vacuum chamber through a brazed ceramic high voltage bushing. The design, illustrated in Figure 5.8, is of the brazed ceramic-to-metal type with a copper gasketed flange for mounting on the vacuum envelope. The cable terminations on the bushing are shielded by a corona ring to reduce leakage currents. The high voltage bushing will be enclosed in an "O"-ring sealed steel chamber which can be evacuated and backfilled with SF₆.

(U) The cables terminate at the SF₆ tank by flaring the cable shield in a bell shape, which is potted with a silastic rubber. Tests to 250 kV, the limit of present power supplies, were performed, with no voltage breakdown, and reliable operation to 300 kV is expected. This method of gun-power supply connection and termination on the gun should prevent personnel hazards and reduce RFI.

5.4 Power Supplies. (U) The HV power supply system, which has been specifically designed to provide power to the large area cathode electron gun, will include a cathode heater isolation transformer, energy storage bank, grid voltage bias and pulser circuit, safety dump, and 300 kV dc charging power supply. The controller will include cabinet, appropriate controls and interconnecting cables. The HV supply, isolation transformer, energy storage, safety dump and grid pulser circuit will be located in a common oil filled tank. Three HV cable sockets will be provided on the tank lid for termination of the negative HV dc, cathode heater power and grid pulse. The power supply grid pulser and isolation transformer controls will be located in a separate equipment rack cabinet and suitable interconnecting cables will be provided.

UNCLASSIFIED

6.0 REFERENCES (U)

1. W. Q. Jeffers and J. D. Kelley, "Calculations of VV Transfer Probabilities in CO-CO Collisions," *J. Chem. Phys.* 55, 4433, 1971.
2. Northrop Report NLSD 71-2R, "Characteristics of a CO Laser," M. L. Bhaumik, November 1971.
3. Northrop Report NLSD 71-7R, "CO Laser Line Selection Technique," M. L. Bhaumik, December 1971. (AD 734 417)
4. Northrop Report NLSD 71-8R, "Quarterly Technical Status Report, High Power CO Laser," December 1971 (AD 518 509).
5. Northrop Report NLSD 72-7R, "Semi Annual Report, High Power CO Laser," March 1972 (AD 520 202).
6. Northrop Report NLSD 72-8R, "Electron Density in an Electron Beam Stabilized High Pressure Discharge," B. B. O'Brien, March 1972.
7. Northrop Report NLSD 72-11R, "Absorption Measurements of Carbon Monoxide Laser Radiation by Water Vapor," D. K. Rice, July 1972.
8. Northrop Report NLSD 72-13R, "Monochromatic Loss Measurements for a Carbon Monoxide Laser Utilizing an Intracavity Vapor Absorption Cell," D. K. Rice, August 1972.
9. M. L. Bhaumik, "CO Laser Line Selection Technique for High Atmospheric Transmission," *Appl. Phys. Lett.*, Vol. 20, No. 9, pp 342-344, 1 May 1972.
10. W. B. Lacina, M. M. Mann, M. L. Bhaumik and G. Hasserjian, "High Power CO Laser," presented at Fifth DOD Conference on Laser Technology, US Naval Postgraduate School, Monterey, California, April 1972, to be published in Conference Proceedings.
11. W. B. Lacina and M. M. Mann, "Transient Oscillator Analysis of a High Pressure Electrically Excited CO Laser," to be published *Applied Physics Letters* September 1972.

UNCLASSIFIED

12. D. K. Rice, "Absorption Measurements of Carbon Monoxide Laser Radiation by Water Vapor," to be published in Appl. Opt. February 1973.
13. M. L. Bhaumik, W. B. Lacina and M. M. Mann, "Characteristics of a CO Laser," IEEE J. Quant. Elect. QE-8, 150, 1972.
14. Northrop Report NCL 71-32R, "Kinetic Model and Theoretical Calculations for Steady State Analysis of Electrically Excited CO Laser Amplifier System," W. B. Lacina, August 1971.
15. W. L. Nighan, "Electron Energy Distributions and Collision Rates in Electrically Excited N₂, CO and CO₂," Phys. Rev., 2A, 1989, 1970.
16. J. T. Yardley, "Vibrational Energy Transfer in CO-He Lasers," J. Chem. Phys. 52, 3983, 1970.
17. G. Hancock and I. W. M. Smith, "Quenching of Infrared Chemiluminescence," Appl. Optics, Special Issue, August 1971.
18. C. Wittig and I. W. M. Smith, "Vibrational Relaxation of Carbon Monoxide ($4 \leq v \leq 10$) at T 100°K," submitted for publication.
19. R. A. McClatchey, "Atmospheric Attenuation of CO Laser Radiation," AD 729 447, July 1971.
20. R. A. McClatchey, AFCRL Optical Physics Laboratory, private communication.

Security Classification

DOCUMENT CONTROL DATA - R & D

Security classification of title, body of abstract and indexing annotation must be entered when the overall report is classified)

1. ORIGINATING ACTIVITY (Corporate author)
Northrop Corporation, Research and Technology Center
Laser Technology Laboratories

2A. REPORT SECURITY CLASSIFICATION
SECRET

2B. GROUP
3

3. REPORT TITLE
Third Quarterly Technical Status Report, High Power CO Laser (U)

4. DESCRIPTIVE NOTES (Type of report and inclusive dates)
Third Quarterly Technical, March through May 1972

5. AUTHOR(S) (First name, middle initial, last name)
Laser Technology Laboratories

6. REPORT DATE
July 1972

7A. TOTAL NO. OF PAGES
80

7B. NO. OF REFS
20

8A. CONTRACT OR GRANT NO.
N00014-72-C-0043

8B. PROJECT NO.
C.
d.

9A. ORIGINATOR'S REPORT NUMBER(S)
NLSD 72-14R

9B. OTHER REPORT NUMBER (Any other numbers that may be assigned this report)
None

10. DISTRIBUTION STATEMENT
[REDACTED]

11. SUPPLEMENTARY NOTES
None

12. SPONSORING MILITARY ACTIVITY
Advanced Research Projects Agency,
ARPA Order No. 1806

13. ABSTRACT
(U) The third quarter effort on the High Power CO Laser Program is reviewed. The program is directed toward the development of the required CO laser technology, the required component technology and the design and construction of intermediate power laser devices. The results of analytical and experimental investigation of the basic characteristics of the laser and data from a high pressure electrically excited CO laser device are discussed.

KEY WORDS	LINK A		LINK B		LINK C	
	ROLE	WT	ROLE	WT	ROLE	WT
CO Laser Molecular Lasers Electrical Discharge Lasers High Power Lasers						



DEPARTMENT OF THE NAVY
OFFICE OF NAVAL RESEARCH
800 NORTH QUINCY STREET
ARLINGTON, VA 22217-5660

IN REPLY REFER TO

5510/1
Ser 93/804
26 Aug 98

From: Chief of Naval Research
To: Defense Technical Information Center
ATTN: Bill Bush, DTIC-OCQ
8725 John J. Kingman Road Suite 0944
Ft. Belvoir, VA 22060-6218

Subj: DECLASSIFICATION OF ONR DOCUMENTS

1. The following documents have been declassified by authority of the Chief of Naval Research and assigned Distribution Statement A:

~~AD 518 509~~

~~AD 520 202~~

AD 522 005 ✓

2. Questions may be directed to the undersigned on (703) 696-4619.

PEGGY LAMBERT
By direction

*Completed
10 Jul 2000
S.W.*